

Published in IEEE Access with doi: 10.1109/ACCESS.2022.3142742

© 2022. This manuscript version is made available under the CC-BY-NC-ND 4.0 license <https://creativecommons.org/licenses/by-nc-nd/4.0/>

Date of publication xxxx 00, 0000, date of current version xxxx 00, 0000.

Digital Object Identifier 10.1109/ACCESS.2022.3142742

# COOT BIRD ALGORITHMS BASED TUNING PI CONTROLLER FOR OPTIMAL MICROGRID AUTONOMOUS OPERATION

Ahmed M. Hussien<sup>1</sup>, Rania A. Turkey<sup>1</sup>, Abdulaziz Alkuhayli<sup>2</sup>, Hany M. Hasanien<sup>3</sup>, Senior Member, IEEE, Marcos Tostado-Véliz<sup>4</sup>, Francisco Jurado<sup>4</sup>, Senior Member, IEEE, and Ramesh C. Bansal<sup>5</sup>

<sup>1</sup>Electrical Engineering Department, Faculty of Engineering and Technology, Future University in Egypt, Cairo, Egypt, 11835. (e-mails: [ahmed.moreab@fue.edu.eg](mailto:ahmed.moreab@fue.edu.eg), [Rania.turky@fue.edu.eg](mailto:Rania.turky@fue.edu.eg))

<sup>2</sup>Electrical Engineering Department, College of Engineering, King Saud University, Riyadh 11421, Saudi Arabia.

<sup>3</sup>Electrical Power and Machines Department, Faculty of Engineering, Ain Shams University, Cairo 11517, Egypt. (e-mails: [hanyhasanien@ieec.org](mailto:hanyhasanien@ieec.org))

<sup>4</sup>Department of Electrical Engineering, Superior Polytechnic School of Linares, University of Jaén, 23700 Linares, Spain.

<sup>5</sup>Electrical Engineering Department, University of Sharjah, Sharjah, United Arab Emirates, and Department of Electric, Electronic and Computer Engineering, University of Pretoria, Pretoria, South Africa

Corresponding author: Ahmed Moreab Hussien ([ahmed.moreab@fue.edu.eg](mailto:ahmed.moreab@fue.edu.eg))

**ABSTRACT** This paper develops a novel methodology for optimal control of islanded microgrids (MGs) based on the coot bird metaheuristic optimizer (CBMO). To this end, the optimum gains for the PI controller are found using the CBMO under a multi-objective optimization framework. The Response Surface Methodology (RSM) is incorporated into the developed procedure to achieve a compromise solution among the different objectives. To prove the effectiveness of the new proposal, a benchmark MG is tested under various scenarios, 1) isolate the system from the grid (autonomous mode), 2) islanded system exposure to load changes, and 3) islanded system exposure to a 3 phase fault. Extensive simulations are performed to validate the new method taking conventional data from PSCAD/EMTDC software. The validity of the suggested optimizer is proved by comparing its results with that achieved using the LMSRE-based adaptive control, sunflower optimization algorithm (SFO), Ziegler-Nichols method and the particle swarm optimization (PSO) techniques. The article shows the superiority of the suggested CBMO over the LMSRE-based adaptive control, SFO, Ziegler-Nichols and the PSO techniques in the transient responses of the system.

**INDEX TERMS** distributed generators; sunflower optimization algorithm; microgrid; renewable energy; coot bird metaheuristic optimizer.

## I. INTRODUCTION

### A. LITERATURE SURVAY

Because of the ever-increasing demand for electric energy and growing environmental concern about pollution and greenhouse gas emissions, the energy market is increasingly embracing distributed energy resources (DERs) such as fuel cells, photovoltaic (PV) systems, micro-turbines, wind farms, etc. [1–4]. Most of the DER-based distributed generators (DGs) are connected to the electric grid using voltage source inverters (VSIs) [5]. These inverter-based DGs have entirely different physical properties than traditional synchronous generators (SGs). As a result, various control techniques for VSIs based on DGs are necessary for desired control action. The SG, for example, has a high inertia because of its huge spinning mass, which contributes to grid stability by sustaining the grid frequency. The lack of inertia and rotational mass in DGs creates technical difficulties, such as the requirement for storage units and suitable regulatory systems to maintain grid stability. As a result, the concept of the microgrid (MG) is being promoted.

The MG is a controlled structure made up of numerous DG units, loads, and storage facilities that are all tied to a local network. The MG can be operated in off-grid or in grid-connected modes [6]. MGs are frequently located near loads to reduce the transmission losses, offer reliable power supply and permit several RESs to collaborate in a distributed form, leading to greater supply security. The grid sets the operating voltage and frequency in the grid-connected mode. On the other hand, the VSI has to maintain these functions in islanded mode [7-9]. In this regard, the control of VSI interfaces becomes more difficult [10-11].

Advanced control systems are therefore employed in off-grid mode to guarantee applicable and reliable operation. These control systems are grouped into 3 classes, droop-based control, centralized control, and multivariable and servomechanism (MVAS) techniques. Droop control is utilized in relying on SG droop characteristics, to offer peer-to-peer control and plug-and-play features by independently managing the power output of separate DG units without the need for interaction or coordination among

DGs. A wireless control strategy concentrated on P-Q droop management has been recommended [12]. In [13], a complete decentralized method relying on dual-frequency-droop control is offered. The capacity of autonomously regulate distributed units without interaction among them is one of the advantages of utilizing droop-based control. This scheme outperforms other power-sharing and MG frequency regulation methods in terms of robustness and consistency. But, for low voltage MGs with resistor line impedance, droop control efficiency is strongly impacted by line impedance, leading to power couplings [14]. The virtual vector transformation technique has been enhanced [15] to evade power coupling, but it reduces the stability of the system. On the contrary, centralized control techniques need high bandwidth interconnections and any breakdown of such links might result in a microgrid failure. In [16], A centralized control system for DC MG based on autonomous communication has been designed and deployed. To end with, a novel approach for developing multivariable resilient servomechanism systems for multi-input multi-output open-loop stable systems has been suggested in [17]. Unfortunately, its great complexity is a burden.

For nonlinear problems, it is found that the most frequently applied controller is the proportional-integral (PI) scheme due to its great stability margin. Unfortunately, it struggles with parameter fluctuation sensitivity and network nonlinearity. As a result, determining the appropriate PI controller settings in this nonlinear system is a significant problem.

## B. RESEARCH GAP AND MOTIVATION

In the past few years, extensive research has been done to design the optimum controller for MG systems to assure successful performance. In this regard, PI controllers maintain the voltage source converter (VSC) voltage with the aid of a d-q frame [18]. PI controllers are regulated using simple approaches like the Ziegler-Nichols [19] method when assuming linearity of the system. Conversely, the PI controller creates a saturation outcome, decreasing the control stability margin as a result of a more significant phase lagging. Controllers are frequently responsive to changes in parameters and operating conditions [20]. In [21], a distributed PI controller to regulate a hybrid power system P&Q is presented. Subsequent, numerous optimization techniques, including particle swarm optimization (PSO) [22], Heap optimization algorithm (HOA) [23], genetic algorithm (GA) [24], sunflower optimization algorithm (SFO) [25], hybrid firefly and particle swarm optimization technique [26], Salp swarm algorithm [27], hybrid GWO-PSO optimization technique [28], hybrid cuckoo search algorithm and grey wolf optimizer (CSA-GWO) [29], equilibrium optimization algorithm (EO) [30], and Whale Optimization Algorithm (WOA) [31], have been used in the MG to enhance decentralized controllers. As reported in

[32], these approaches have however advantages and disadvantages, being still so far to get a universal framework for MG control.

This paper contributes to this pool by developing a novel methodology for optimal control of islanded MGs based on the coot bird metaheuristic optimizer (CBMO). In this research, this optimizer is used in a PI controller optimal control scheme with various PI controller gains to enhance the efficacy of the islanding microgrid operation. Furthermore, the Response Surface Methodology (RSM) is considered to attain a compromise solution among objectives under a multi-objective optimization paradigm. To validate the new proposal, various simulations are carried out to show the superiority of the suggested CBMO in the transient responses of the system over Ziegler-Nichols and some other optimization techniques, such as the LMSRE-based adaptive control, SFO and the PSO techniques.

## C. CONTRIBUTION AND PAPER BODY

To cover the gaps previously exposed, this article contributes with:

- 1) Developing a novel methodology based on CBMO to adjust PI controllers to improve the efficiency of the MG system,
- 2) Evaluate the reliability of the suggested optimizer through experiment the MG under various operating modes, i) cut the system off the grid (autonomous mode), ii) islanded system interrupted by a load changes, and iii) islanded system interrupted by a 3 phase fault,
- 3) Proving the validity of the offered optimizer through comparing its results with that achieved using the LMSRE-based adaptive control, SFO and, Ziegler-Nichols the PSO techniques.

The leftover sectors of the article are ordered in this way. Sector II demonstrates the MG demonstrating. Sector III explains the control plan. Sector IV shows the design procedures. Sector V shows the modelling stage of the Response Surface Methodology (RSM), SFO, LMSRE adaptive control, Ziegler-Nichols and the CBMO. Sector VI introduces the simulation results and discussion. Lastly, the conclusion is introduced in Sector VII.

## II. MG DEMONSTRATING

Fig. 1 depicts a single line diagram of a benchmark MG, which is mainly divided into three DGs linked together via transmission lines. The utility grid is connected to the DGs via a point of common coupling (PCC) through transmission lines. The single DG is made up of a DC supply connected to pulse width modulation (PWM) (2 levels), which is linked to a delta-star transformer via a filter to avoid power quality issues. To represent the local load, RLC load is inserted after

the  $\Delta$  - Y transformer. The MG information is listed in Table 1.

TABLE 1. MG Data

Transformer data		$\Delta/Y = 0.6/13.8$ KV	
Load data	Load 1	$C_1 = 50\mu\text{F}, R_{11} = 9\Omega, R_{12} = 150\Omega, L_1 = 0.6$ H	
	Load 2	$C_2 = 42\mu\text{F}, R_{22} = 5\Omega, R_{12} = 75\Omega, L_2 = 0.4$ H	
	Load 3	$C_3 = 33\mu\text{F}, R_{33} = 20\Omega, R_{12} = 50\Omega, L_3 = 1.5$ H	
Transmission Line parameters	TL1	$R_{TL1} = 0.7 \Omega,$	$L_{TL1} = 0.5$ mH
	TL2	$R_{TL2} = 1.5 \Omega,$	$L_{TL2} = 0.9$ mH
Filter data		$R_f = 1.5$ m $\Omega,$	$X_f = 0.5$ mH
Grid parameters		$V = 13.8$ KV,	$R_g = 0.2 \Omega, L_g = 0.3$ mH

The study MG can be operated either in grid-connected or in stand-alone mode. The DG operates in power control mode when connected to the grid. It is worthy to note that the grid sustains the voltage and frequency. Conversely, in the off-grid mode, the DG is in charge of balancing demands and generation. Moreover, it adjusts the voltage and frequency to sustain them inside acceptable ranges. This study focuses on improving the MG under off-grid operating mode by employing the cascaded control method, which is detailed in the following sector.

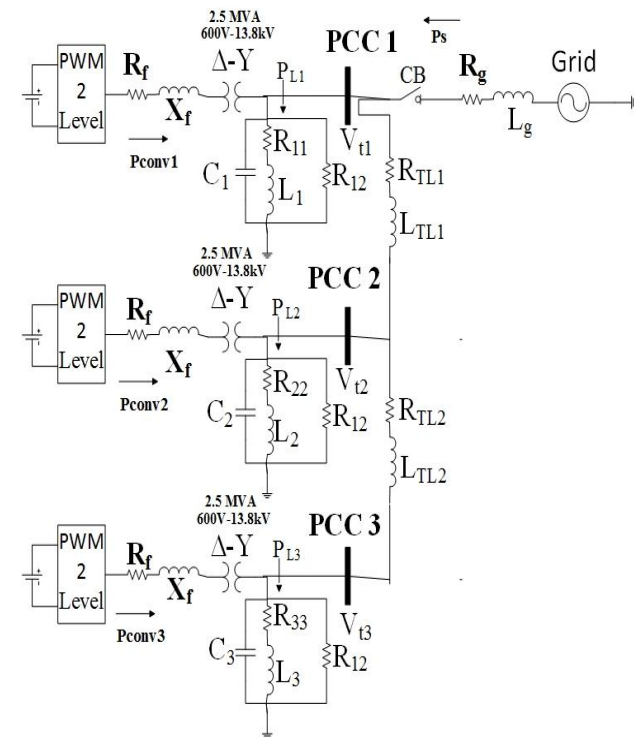


FIGURE 1. Single line diagram of a benchmark MG

### III. CONTROL PLAN

In each DG, the cascaded control scheme is used to stabilize the voltage at the PCC. The reference voltages

( $V_{conv\_a}^*, V_{conv\_b}^*, V_{conv\_c}^*$ ) are achieved by the Inverse Clarke Transformation of the d-q reference voltages ( $V_{conv\_d}^*, V_{conv\_q}^*$ ) and the transformation angle ( $\theta_{PLL}$ ).  $V_{conv\_d}^*$  and  $V_{conv\_q}^*$  are given with the aid of the 4 PI controllers as seen in Fig. 2.  $\theta_{PLL}$  is taken from the phase-locked loop by taking the data of the voltages of the grid in the inputs. The inverter switches pulses are achieved with the aid of the comparator that compares a 1980 Hz (60 HZ multiples) triangular signal and the reference voltages ( $V_{conv\_a}^*, V_{conv\_b}^*, V_{conv\_c}^*$ ).

The gains of the 4 PI controllers are determined using the CBMO method and other optimization techniques. Section IV goes into further depth on this.

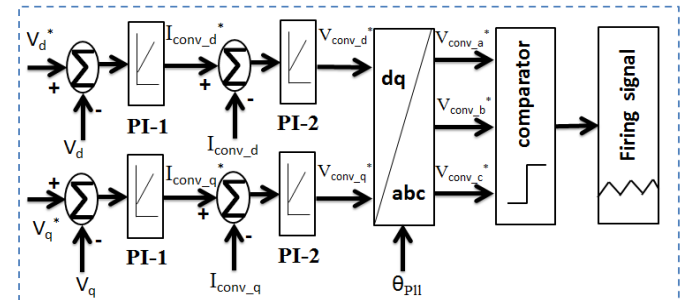


FIGURE 2. control system for off-grid mode

### IV. DESIGN PROCEDURES

#### A. Selection of Variables

In this article, six PI controllers are employed in 3 DGs, two in for each DG, where:

- $PI_{1.1}$  and  $PI_{1.2}$  are the PI controllers utilized in DG<sub>1</sub>,
- $PI_{2.1}$  and  $PI_{2.2}$  are the PI controllers utilized in DG<sub>2</sub> and
- $PI_{3.1}$  and  $PI_{3.2}$  are the PI controllers utilized in DG<sub>3</sub>

The proportional gain (KP) and integral time constants (TI) are the gains for the PI controllers in this research where:

- $Y_1$  is the KP of the  $PI_{1.1}$  in DG<sub>1</sub>,
- $Y_2$  is the TI of the  $PI_{1.1}$  in DG<sub>1</sub>,
- $Y_3$  is the KP of the  $PI_{1.2}$  in DG<sub>1</sub>,
- $Y_4$  is the TI of the  $PI_{1.2}$  in DG<sub>1</sub>,
- $Y_5$  is the KP of the  $PI_{2.1}$  in DG<sub>2</sub>,
- $Y_6$  is the TI of the  $PI_{2.1}$  in DG<sub>2</sub>,
- $Y_7$  is the KP of the  $PI_{2.2}$  in DG<sub>2</sub>,
- $Y_8$  is the TI of the  $PI_{2.2}$  in DG<sub>2</sub>,
- $Y_9$  is the KP of the  $PI_{3.1}$  in DG<sub>3</sub>,
- $Y_{10}$  is the TI of the  $PI_{3.1}$  in DG<sub>3</sub>,
- $Y_{11}$  is the KP of the  $PI_{3.2}$  in DG<sub>3</sub> and
- $Y_{12}$  is the TI of the  $PI_{3.2}$  in DG<sub>3</sub>.

In this article, three levels are utilized for the controllers' variables, which are summarized in Table 2.

- Level -1 is the minimum safe value,
- Level 0 is the average value between Level 1 and -1 and
- Level 1 is the maximum safe value.

TABLE 2. RSM levels

Design variable level	Level (-1)	Level (0)	Level (1)
Y <sub>1</sub>	2	4.75	7.5
Y <sub>2</sub>	0.0009	0.01045	0.02
Y <sub>3</sub>	1.6	2.3	3
Y <sub>4</sub>	0.05	1.525	3
Y <sub>5</sub>	1.5	4.25	7
Y <sub>6</sub>	0.0009	0.00795	0.015
Y <sub>7</sub>	1.4	1.95	2.5
Y <sub>8</sub>	0.05	1.425	2.8
Y <sub>9</sub>	1	3.75	6.5
Y <sub>10</sub>	0.0009	0.00545	0.01
Y <sub>11</sub>	1.2	1.65	2.1
Y <sub>12</sub>	0.05	1.275	2.5

### B. PSCAD/EMTDC PROGRAM

PSCAD software is used to simulate the MG system. The information extracted from these simulations in various scenarios is utilized to be the inputs of the RSM.

### C. THE RSM & MINITAB SOFTWARE

The RSM is a mathematical procedure that empirically creates models by utilizing a good statistical approach to detect correlations between control and dynamic behaviour [33]. The steady-state error (E<sub>ss</sub>), maximum percentage under/overshoots (MPUS/MPOS), and settling time (T<sub>set</sub>) of the reference voltage are the RSM input data which are extracted from PSCAD and presented in Table A1, Table A2, and Table A3 in the Appendix. The RSM is constructed with the aid of MINITAB software.

The multi-objective function for this system is defined by the minimization of the MPOS (N1), MPUS (N2), T<sub>set</sub> (N3), and E<sub>ss</sub> (N4) for the given scenarios. Eq. (1) depicts the second order polynomial RSM model.

$$N_i = M_1 + M_2 Y_1 + M_3 Y_2 + M_4 Y_3 + M_5 Y_4 + M_6 Y_1^2 + M_7 Y_2^2 + M_8 Y_3^2 + M_9 Y_4^2 + M_{10} Y_1 Y_2 + M_{11} Y_1 Y_3 + M_{12} Y_1 Y_4 + M_{13} Y_2 Y_3 + M_{14} Y_2 Y_4 + M_{15} Y_3 Y_4 \quad (1)$$

where i=1, 2, 3, 4, and M<sub>1</sub>, M<sub>2</sub>, ..., M<sub>15</sub> are the computed RSM coefficients for the scenarios are reported in Table A4, Table A5, and Table A6 in the Appendix.

### V. OPTIMIZATION STAGE:

Eq. (1) relies on the weighting technique [34] is utilized as an input to the CBMO, SFO, and PSO techniques to achieve the optimum PI gains that reduce the transients. The

weights utilized in the multi-objective function are listed in Table 3.

TABLE 3. The input weights

Weight (Wt)	location		Value
Wt <sub>1</sub>	DG1	MPUS	0.2
Wt <sub>2</sub>		MPOS	0.2
Wt <sub>3</sub>		T <sub>set</sub>	0.075
Wt <sub>4</sub>		E <sub>ss</sub>	0.03
Wt <sub>5</sub>	DG2	MPUS	0.125
Wt <sub>6</sub>		MPOS	0.125
Wt <sub>7</sub>		T <sub>set</sub>	0.04
Wt <sub>8</sub>		E <sub>ss</sub>	0.02
Wt <sub>9</sub>	DG3	MPUS	0.075
Wt <sub>10</sub>		MPOS	0.075
Wt <sub>11</sub>		T <sub>set</sub>	0.025
Wt <sub>12</sub>		E <sub>ss</sub>	0.01

### A. THE SFO ALGORITHM

The advancement of soft computing capability is the primary impetus for using SFO in the optimization of various issues. The SFO is a natural-motivated heuristic method. Its basic concept is to simulate the configuration of sunflowers to gather sunlight [25]. Daily basis, the sunflower pattern is replayed, started in the sunrise tracking the sunlight and ending in the sundown. The sunflower back into its original place in the evening, waiting for the sun to appear. Each sunflower is thought to have only one pollen gamete. Radiation from the inverse square rule is critical in this case. Because sunflowers absorb a tremendous quantity of energy from the sun relative to those further away. The sunflowers near to the sun tilt toward calm in this location [25]. Eq. (2) indicates the heat absorbed by each population.

$$H_s = \frac{W}{4\pi r_s^2} \quad (2)$$

where W is the power source, and r<sub>s</sub> denotes the distance between the most frequent best and population i. Eq. (3) illustrates the movement of sunflowers [13], while the movement of sunflowers in the direction of "m" is given by Eq. (4).

$$\vec{m}_i = \frac{z^* - z_i}{||z^* - z_i||}, \quad i = 1, 2, \dots, n_p \quad (3)$$

$$d_i = A \times P_i(z_i + z_{i-1}) \times ||z_i + z_{i-1}|| \quad (4)$$

where z is the population, z\* is the best population, n<sub>p</sub> is the population number, A is a constant that characterizes the "inertial" motion of the sunflowers and P<sub>i</sub>(||z<sub>i</sub> + z<sub>i-1</sub>||) is

the pollination possibility. Eq. (5) specifies the constraint of these phases:

$$R_{max} = \frac{\|Z_{max} - Z_{min}\|}{2 \times n_p} \quad (5)$$

where  $Z_{max}$  and  $Z_{min}$  are the minimum and maximum boundaries, respectively. The following plant is defined as follows.

$$\vec{Z}_{i+1} = \vec{Z}_i + d_i \times \vec{m}_i \quad (6)$$

For the sake of clarity, the overall procedure of SFO is summarized in the flowchart of Fig. 3, while the results for this algorithm were taken from [6].

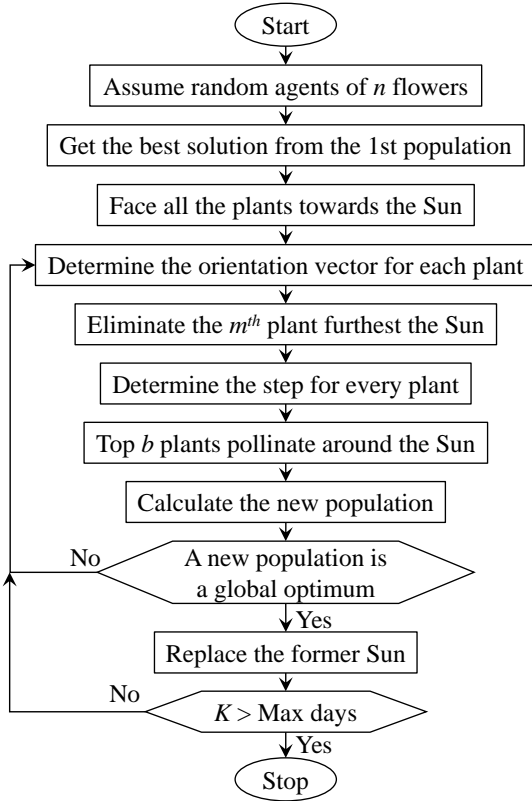


FIGURE 3. Flowchart of SFO algorithm

## B. LMSRE ALGORITHM

The adaptive filtering algorithms (AFAs) are normally utilized to discover the impulse response weight vector ( $G_0$ ) filter [35], as represented in Fig. 4. The input  $F_q$  is implemented as a Gaussian noise  $N_q$  going over FIR filter. Consequently, it depends on the error  $e_q$ .

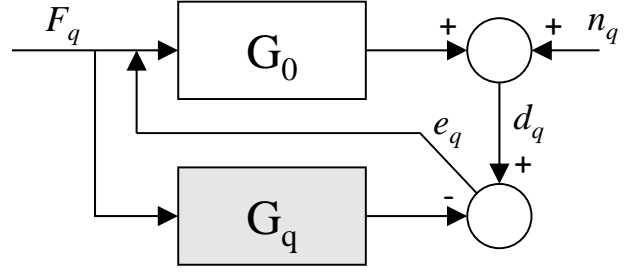


FIGURE 4. System prototypal of FIR filter

The AFAs are iterated using the steepest descent technique, as indicated in Eq (7).

$$G_{q+1} = G_q - \mu \nabla_{G_j}(G_q) \quad (7)$$

where  $q$  is the iteration number and  $W_q$  expresses the estimated vector of the weight. Next, the gradient of the cost function is achieved from Eq. (8).

$$\nabla_{G_j}(G_q) = \text{sign}(e_q) \cdot (-F_q) - \left[ \frac{\exp(-|e_q|)}{\sqrt{1+\exp(-|e_q|)}} \right] \quad (8)$$

By substituting Eq. (7) into Eq. (8) one obtains

$$G_{q+1} = G_q - \mu_q \beta_q \text{sign}(e_q) \cdot F_q \quad (9)$$

where  $\mu_q$  is set to bound the errors. For instance, for the giant error,  $\mu_q$  must be large for quick convergence. Conversely, for a minor error,  $\mu_q$  needs to be reduced. So,  $\beta_q$  diverges from  $[0, 1]$ , and is reduced for small errors and vice versa. Therefore,  $\mu_q$  diverges proportionately to the  $\beta_q$  which stated in eq.(10).

$$\mu_q = \mu \beta_q^{\alpha-1} \quad (10)$$

where  $\mu$  and  $\alpha$  are in control of deviation of  $\mu_q$ . Then, replacing Eq. (9) into Eq. (10) yields

$$G_{q+1} = G_q - \mu \beta_q^\alpha \text{sign}(e_q) \cdot F_q \quad (11)$$

The LMSRE method is used to modify the PI Controller methods that rely on eq (11). The following are the adjusted PI parameters:

$$k_{p(q+1)} = k_{p(q)} + \Delta k_{p(q)} \quad (12)$$

$$T_{i(q+1)} = T_{i(q)} + \Delta T_{i(q)} \quad (13)$$

$$\Delta k_{p(q)} = \Delta T_{i(q)} = \mu \beta_q^\alpha \text{sign}(e_q) \cdot F_q \quad (14)$$

The opening PI gains ( $k_p$  and  $T_i$ ) for the six PI controllers (PI<sub>1.1</sub> to PI<sub>3.2</sub>) are achieved manually by testing the system in its boundaries, where stated in Table 4. The outputs of LMSRE were taken from [6].

**TABLE 4. The initial LMSRE PI gains**

controller	PI <sub>1,1</sub>	PI <sub>1,2</sub>	PI <sub>2,1</sub>	PI <sub>2,2</sub>	PI <sub>3,1</sub>	PI <sub>3,2</sub>
initial k <sub>p</sub>	5.5	3	5.5	3	5.5	3
initial T <sub>i</sub>	0.003	0.3	0.003	0.3	0.003	0.3

### C. ZIEGLER-NICHOLS

A conventional control technique for fine-tuning PI gains named Ziegler–Nichols is presented. This technique initiates by zeroing the K<sub>p</sub> and T<sub>i</sub>, then increases the K<sub>p</sub> until the system critically stable. The K<sub>p</sub> at this point named K<sub>cr</sub> and the critical period named P<sub>cr</sub>. The PI gains are determined according to Table 5 [36].

**TABLE 5. Rules for PI Gains based on Ziegler–Nichols Technique [36].**

Controller type	K <sub>p</sub>	T <sub>i</sub>	K <sub>d</sub>
P	0.5 K <sub>cr</sub>	Inf.	0
PI	0.45 K <sub>cr</sub>	(1/1.2) P <sub>cr</sub>	0
PID	0.6 K <sub>cr</sub>	0.5 P <sub>cr</sub>	0.125 P <sub>cr</sub>

### D. OPTIMIZATION USING CBMO

The CBMO mimics the behaviour of a group of American coots swimming in a lake [37]. The primary algorithm was developed based on the behaviours of American coots when travelling in a lake, particularly when confronted with excessive waving and environmental conditions [38], [39]. Lukeman et al. examined how to surf scoters change their configurations to travel in line with the big waves. The coots are travelling in a dense flock in front or behind [40]. They organize themselves in two or three dimensions to migrate and change between two phases. The first is an unstructured stage characterized by low density and non-homogeneous coot body directions. However, the other stage is characterized by high density, uniform coot body motions, and velocity. By travelling over a long distance, coots can accelerate their movements in three dimensions.

The coots can move between the first and the second phase utilizing one of two techniques. The first is to accelerate certain nearby coot followers and change their locations so that they are aligned with other coots and enhance the orientations of coot leaders. The second strategy is to promote coot followers with great potential as leaders rather than leaders with poor results. The time necessary to go from one phase to the next is determined by the density of the coots. The coot leaders are calculated as a percentage of the total estimated coot "populations, N<sub>pop</sub>," while the rest are coot followers. The places of followers (Poscoots0)

and leaders (Posleader) are chosen at random as presented in eq. (15-16), respectively.

$$P_{0\text{Scoots}} = \text{Rand}_{\text{coot}} \cdot (U_b - L_b) + L_b \quad (15)$$

$$P_{0\text{Sleader}} = \text{Rand}_{\text{leader}} \cdot (U_b - L_b) + L_b \quad (16)$$

where U<sub>b</sub> denotes the upper limit and L<sub>b</sub> denotes the lower limit. All of Coot's followers' fitness Fit<sub>coots</sub> could be calculated utilizing the OF (F<sub>obj</sub>) as shown in eq. (17).

$$\text{Fit}_{\text{coots}}(1, i) = F_{\text{obj}}(P_{0\text{Scoot}}(i)), \quad i = 1 \text{ to } N_{\text{coots}} \quad (17)$$

where N<sub>coots</sub> is the number of Coot's followers = N<sub>pop</sub> - N<sub>leaders</sub>. Gbest<sub>score</sub> and Gbest<sub>pos</sub> identify the best global coots score and its position, respectively as seen in eq. (18).

$$\left\{ \begin{array}{l} \text{If } G_{\text{best\_score}} > \text{Fit}_{\text{coots}}(1, i) \text{ then} \\ G_{\text{best\_score}} = \text{Fit}_{\text{coots}}(1, i) \ \& \\ G_{\text{best\_pos}} = P_{0\text{Scoot}}(i) \end{array} \right. \quad (18)$$

Furthermore, the OF may be used to assess the fitness of all Coot's leaders by Eq. (19). The Gbest<sub>score</sub> and its position Gbest<sub>pos</sub> are distinguished by eq. (20).

$$\text{Fit}_{\text{leaders}}(1, i) = F_{\text{obj}}(P_{0\text{Sleader}}(i)), \quad i = 1 \text{ to } N_{\text{leaders}} \quad (19)$$

$$\left\{ \begin{array}{l} \text{If } G_{\text{best\_score}} > \text{Fit}_{\text{leaders}}(1, i) \text{ then} \\ G_{\text{best\_score}} = \text{Fit}_{\text{leaders}}(1, i) \ \& \\ G_{\text{best\_pos}} = P_{0\text{Sleader}}(i) \end{array} \right. \quad (20)$$

where N<sub>leaders</sub> is the number of Coot's leaders (% N<sub>pop</sub>).

Each of the Coot's followers is allocated to a Coot leader based on a random process, and their locations are updated appropriately, beginning with iteration two and ending with the maximum number of iterations (IT<sub>max</sub>) as presented in Eqs. (21) and (22). The locations of the new followers are verified to ensure that they are within the parameters specified in Eq. (22).

$$R = 1 + 2 \cdot \text{Rand}_{\text{coots}} \quad (21)$$

$$P_{0\text{Scoot}}(i) = 2 \cdot \text{Rand}_{\text{coots}} \cdot \cos(2\pi R) \cdot [P_{0\text{Sleader}}(k) - P_{0\text{Scoot}}(i)] + P_{0\text{Sleader}}(k), \quad \forall i \in N_{\text{coots}} \text{ and } k \in N_{\text{leaders}} \quad (22)$$

$$\left\{ \begin{array}{l} \text{If } P_{0\text{Scoot}}(i) > U_b, \text{ then, } P_{0\text{Scoot}}(i) = U_b \\ \text{If } P_{0\text{Scoot}}(i) < L_b, \text{ then, } P_{0\text{Scoot}}(i) = L_b \end{array} \right. \quad (23)$$

where Rand<sub>coots</sub> are the randomly produced values of the Coot's followers and Rand<sub>leaders</sub> are the randomly created values of the Coot's leaders.

The new fitness of all Coot's followers is assessed and compared to the fitness of the leader. If a follower fitness exceeds that of its associated leader, the follower becomes a leader, and the leader becomes a follower. This process is shown in Eq. (24).

$$\left\{ \begin{array}{l} \text{If } \text{Fit}_{\text{coots}}(1, i) < \text{Fit}_{\text{leader}}(1, k) \text{ then} \\ \text{Fit}_{\text{leader}}(1, k) = \text{Fit}_{\text{coots}}(1, i) \ \& \\ P_{0\text{Sleader}}(k) = P_{0\text{Scoots}}(i) \end{array} \right. \quad (24)$$

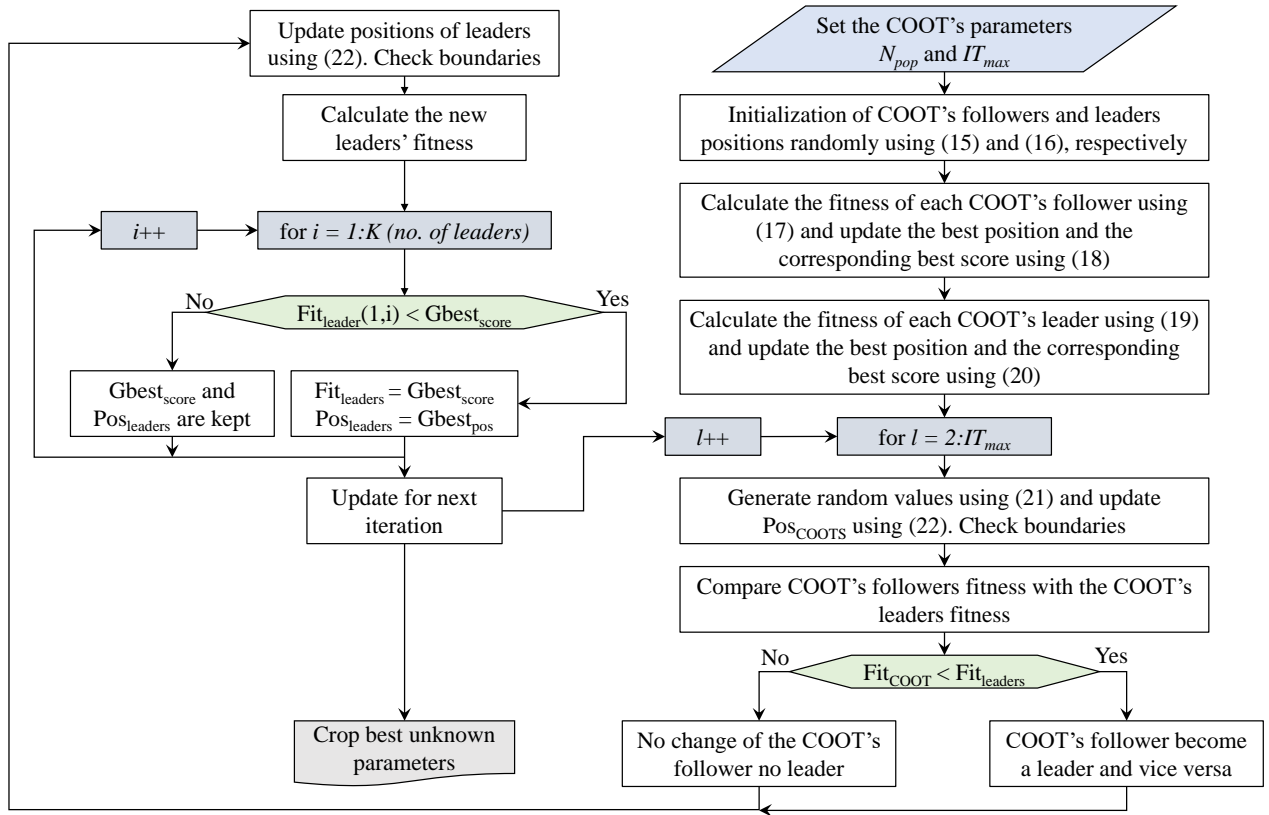


FIGURE 5. Flowchart of CMBO algorithm

The locations of the leaders are enhanced using a random function, as shown in Eqs. (25), and (26).

$$\begin{cases} B = 2 - (IT(L)2/IT_{max} \\ R = 1 + 2 \cdot \text{Rand}_{leaders} \end{cases} \quad (25)$$

$$\begin{cases} P_{0sleaders} = B \cdot \text{Rand}_{leaders} \cdot \cos(2\pi R) \cdot [Gbest_{pos} - \\ P_{0sleaders}(i)] + Gbest_{pos} \end{cases} \quad (26)$$

where  $IT(L)$  denotes the iteration  $L$ . For the sake of summary, the flowchart of CBMO is presented in Fig. 5.

The best global score and position are determined in eq. (27).

$$\begin{cases} \text{If } Gbest_{score} > Fit_{leaders}(1, i) \text{ then} \\ Fit_{leader}(1, k) = Gbest_{score} \ \& \\ P_{0sleaders}(i) = Gbest_{pos} \end{cases} \quad (27)$$

## VI. SIMULATION RESULTS AND DISCUSSION

This sector is devoted on proving numerical results with the aim of demonstrating the validity and efficacy of the proposed control method based on CMBO. As a major indicator, the effectiveness of the new proposal will be evaluated as its capacity to keep the PCC voltage around the specified ranges in different MG operative modes. The

soberness of the controller scheme is demonstrated through the simulation outcomes, where taken from the PSCAD/EMTDC environment. To prove the superiority of the CMBO-based methodology developed, it is compared with the results obtained with the LMSRE-based adaptive control, SFO, Ziegler-Nichols and the PSO techniques reported in [6]. The system has been experimented under different microgrid operating modes, 1) isolate the system from the grid (autonomous mode), 2) islanded system exposure to load changes, and 3) islanded system exposure to a 3-phase fault.

### A. SCENARIO 1 (OFF-GRID MODE)

In the first scenario, the MG run at normal states and connected to the grid. The MG is abruptly separated from the grid (islanding) at time equal to 2 second. The Ziegler-Nichols Critical gains ( $k_{cr}$ ) and Critical periods ( $P_{cr}$ ) for the DGs are reported in Table 6. The optimum PI gains data for the DGs for CBMO, SFO, PSO, Ziegler-Nichols and LMSRE are reported in Table 7. Figs. 6 (a, b, c) depict the reference voltage in the DGs for CBMO, SFO, PSO, Ziegler-Nichols and LMSRE, while Figs. 7 (a, b, c) plot the active



and reactive powers for the load in the DGs for CBMO, SFO, PSO, Ziegler-Nichols and LMSRE. It is worthwhile to note that, in Fig. 6a, the MPUS for the stand-alone mode for the offered technique is less than 7.5%. Moreover, the  $T_{set}$  based on the 2% criterion for the proposed controller is reduced to 4 ms, and the  $E_{ss}$  is 0.29%. Thus, the introduced optimizer offers the least overshoots, quick damping, and applicable  $E_{ss}$ . It is worthy to note that the CBMO is much better in MPUS, MPOS,  $T_{set}$ , and  $E_{ss}$  over LMSRE-based adaptive control, SFO, Ziegler-Nichols and the PSO techniques, which verify the rigidity, validation, and applicability of the presented CBMO over LMSRE-based adaptive control, SFO, Ziegler-Nichols and the PSO techniques.

**TABLE 6.** The Ziegler-Nichols Critical gains ( $k_{cr}$ ) and Critical periods ( $P_{cr}$ ) for the DGs for Scenario1

	Critical gains ( $k_{cr}$ )	Critical periods ( $P_{cr}$ )	PI gains	
			$Y_i$	
$PI_{1,1}$	7.5	0.0048	$Y_1$	3.375
			$Y_2$	0.004
$PI_{2,1}$	3	1.2	$Y_3$	1.35
			$Y_4$	1
$PI_{2,1}$	7	0.00456	$Y_5$	3.15
			$Y_6$	0.0038
$PI_{2,2}$	2.5	1.1856	$Y_7$	1.125
			$Y_8$	0.988
$PI_{3,1}$	6.5	0.00432	$Y_9$	2.925
			$Y_{10}$	0.0036
$PI_{3,2}$	2.1	1.1532	$Y_{11}$	0.945
			$Y_{12}$	0.961

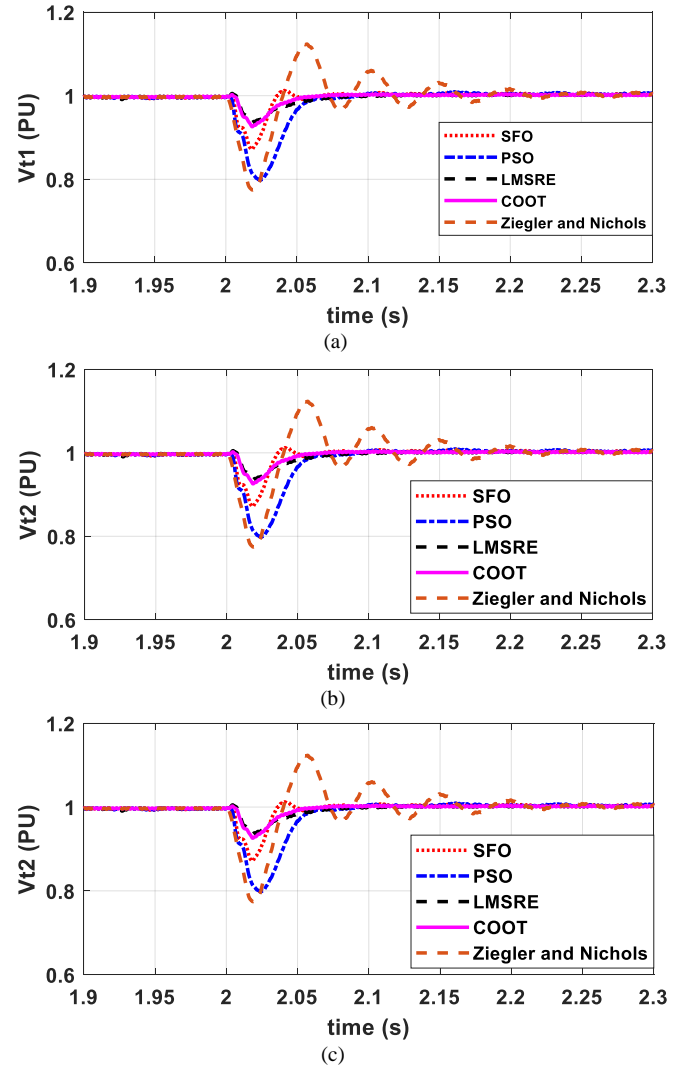


**FIGURE 6.** The Results of CBMO, SFO, PSO, Ziegler-Nichols and LMSRE for Scenario1. (a) Reference voltage of DG 1. (b) Reference voltage of DG 2. (c) Reference voltage of DG 3

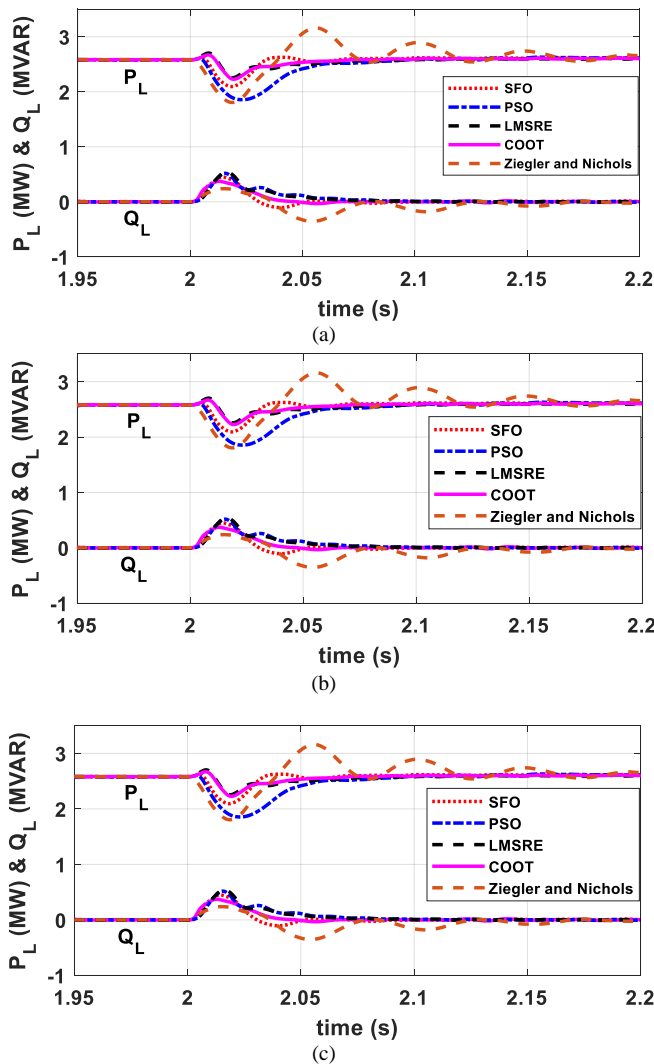


FIGURE 7. The Results of CBMO, SFO, PSO, Ziegler-Nichols and LMSRE for Scenario1. (a) Active and reactive load powers in DG 1. (b) Active and reactive load powers in DG 2. (c) Active and reactive load powers in DG 3.

TABLE 7. Results of CBMO, SFO, PSO, Ziegler-Nichols and LMSRE for Scenario1

Point of compar.	COOT	LMSRE	SFO	PSO	Ziegler-Nichols				
Scenario 1 DG 1									
Optimum size	Y <sub>1</sub>	6.21	online	Y <sub>1</sub>	6.41	Y <sub>1</sub>	2.147	Y <sub>1</sub>	3.375
	Y <sub>2</sub>	0.0321		Y <sub>2</sub>	0.0053	Y <sub>2</sub>	0.0057	Y <sub>2</sub>	0.004
	Y <sub>3</sub>	2.65		Y <sub>3</sub>	2.951	Y <sub>3</sub>	1.679	Y <sub>3</sub>	1.35
	Y <sub>4</sub>	1.91		Y <sub>4</sub>	0.3471	Y <sub>4</sub>	0.339	Y <sub>4</sub>	1
MPUS	7.423 %	7.91%	12.91%	20.261%	22.5 %				
MPOS	zero	zero	zero	zero	12.1 %				
T <sub>set</sub>	0.0382 s	0.0462 s	0.0331 s	0.0541 s	0.165 s				
E <sub>ss</sub>	0.29 %	0.321%	0.351%	0.405%	1.002 %				
Scenario 1 DG 2									
Optimum size	Y <sub>5</sub>	6.15	online	Y <sub>5</sub>	5.981	Y <sub>5</sub>	1.5691	Y <sub>5</sub>	3.15
	Y <sub>6</sub>	0.0318		Y <sub>6</sub>	0.00409	Y <sub>6</sub>	0.0043	Y <sub>6</sub>	0.0038
	Y <sub>7</sub>	2.59		Y <sub>7</sub>	2.5081	Y <sub>7</sub>	1.2341	Y <sub>7</sub>	1.125
	Y <sub>8</sub>	1.95		Y <sub>8</sub>	0.2988	Y <sub>8</sub>	0.3057	Y <sub>8</sub>	0.988
MPUS	7.434 %	7.899%	12.861%	20.11%	22.4 %				
MPOS	zero	zero	zero	zero	11.95 %				
T <sub>set</sub>	0.03827 s	0.0462 s	0.0327 s	0.0536 s	0.166				
E <sub>ss</sub>	0.312 %	0.305%	0.361%	0.406%	0.97 %				
Scenario 1 DG 3									
Optimum size	Y <sub>9</sub>	6.04	online	Y <sub>9</sub>	5.5341	Y <sub>9</sub>	1.068	Y <sub>9</sub>	2.925
	Y <sub>10</sub>	0.0307		Y <sub>10</sub>	0.00312	Y <sub>10</sub>	0.0032	Y <sub>10</sub>	0.0036
	Y <sub>11</sub>	2.51		Y <sub>11</sub>	2.0991	Y <sub>11</sub>	0.993	Y <sub>11</sub>	0.945
	Y <sub>12</sub>	1.99		Y <sub>12</sub>	0.24785	Y <sub>12</sub>	0.2588	Y <sub>12</sub>	0.961
MPUS	7.451 %	7.572%	12.61%	19.976%	22.31%				
MPOS	zero	zero	zero	zero	11.87 %				
T <sub>set</sub>	0.03831 s	0.0433 s	0.0323 s	0.0532 s	0.159 s				
E <sub>ss</sub>	0.289 %	0.311%	0.321%	0.403%	0.95 %				

### B. SCENARIO 2 (LOAD CHANGING)

In the second scenario, the MG run at normal states and in the stand-alone mode. The MG initially operates implemented with RLC loads, where stated in Table 1. R12 is varied from 150 Ω to 300 Ω at t = 3 s and back to its original state at time=3.4 s. The Ziegler-Nichols Critical gains ( $k_{cr}$ ) and Critical periods ( $P_{cr}$ ) for the DGs are reported in Table 8. The optimum PI gains data for the DGs for CBMO, SFO, PSO, Ziegler-Nichols and LMSRE are introduced in Table 9. Figs. 8 (a, b, c) shows the reference voltage in each DG for CBMO, LMSRE, SFO, Ziegler-Nichols and PSO. Figs. 9 (a, b, c) plot the active and reactive powers for the load in the DGs for CBMO, SFO, PSO, Ziegler-Nichols and LMSRE. It is worthy to note that, in Fig. 8a, the MPUS and MPOS for the load variability scenario for the offered technique are below 1%. Furthermore, the T<sub>set</sub> relies on the 2% criterion for the proposed controller is reduced to zero seconds, and the E<sub>ss</sub> is 0.38%. Thus, the

introduced optimizer offers the least overshoots, quick damping, and applicable  $E_{ss}$ . It is worthy to recognize that, in Fig. 8a, the real load power of DG 1 is reduced from 2.6 MW to 0.5 MW and restored to its original value efficiently at  $t=3.4$  s. Alternatively, the real load powers for the rest DGs have quick damping with lesser oscillations. It is worthy to note that the CBMO is much better in MPUS, MPOS,  $T_{set}$ , and  $E_{ss}$  over LMSRE-based adaptive control, SFO, Ziegler-Nichols and the PSO techniques, which verify the rigidity, validation, and applicability of the presented CBMO over LMSRE-based adaptive control, SFO, Ziegler-Nichols and the PSO techniques.

**TABLE 8.** The Ziegler-Nichols Critical gains ( $k_{cr}$ ) and Critical periods ( $P_{cr}$ ) for the DGs for Scenario2

	Critical gains ( $k_{cr}$ )	Critical periods ( $P_{cr}$ )	PI gains	
			$Y_1$	$Y_2$
PI <sub>1,1</sub>	3.33	0.01056	$Y_1$	1.5
			$Y_2$	0.0088
PI <sub>2,1</sub>	3.556	0.1896	$Y_3$	1.6
			$Y_4$	0.158
PI <sub>2,1</sub>	2.1889	0.01032	$Y_5$	0.985
			$Y_6$	0.0086
PI <sub>2,2</sub>	3.444	0.186	$Y_7$	1.55
			$Y_8$	0.155
PI <sub>3,1</sub>	2.1556	0.00984	$Y_9$	0.97
			$Y_{10}$	0.0082
PI <sub>3,2</sub>	3.3778	0.1812	$Y_{11}$	1.52
			$Y_{12}$	0.151

**C. SCENARIO 3 (3-PHASE FAULT)**

In scenario 3, the MG run at normal states and in the stand-alone mode. Then, a 3-phase fault is applied at PCC 1 at  $t=4$  s, and the fault is removed at  $t=4.1$  s. The Ziegler-Nichols Critical gains ( $k_{cr}$ ) and Critical periods ( $P_{cr}$ ) for the DGs are reported in Table 10. Table 11 introduces the optimum PI gains data in the DGs for CBMO, SFO, PSO, Ziegler-Nichols and LMSRE. Figs. 10 (a, b, c) plot the reference voltage in the DGs for CBMO, LMSRE, SFO, Ziegler-Nichols and PSO. Figs. 11 (a, b, c) show the active and reactive powers for the load in each DG for CBMO, SFO, PSO, Ziegler-Nichols and LMSRE. It is worthy to note that, in Fig. 10a, the  $T_{set}$  relies on the 2% criterion for the offered optimizer is 24 ms, and the  $E_{ss}$  is 0.31%. Thus, the introduced optimizer offers quick damping and applicable  $E_{ss}$ . which verify the rigidity, validation, and applicability of the presented CBMO over LMSRE-based adaptive control, SFO, Ziegler-Nichols and the PSO techniques.

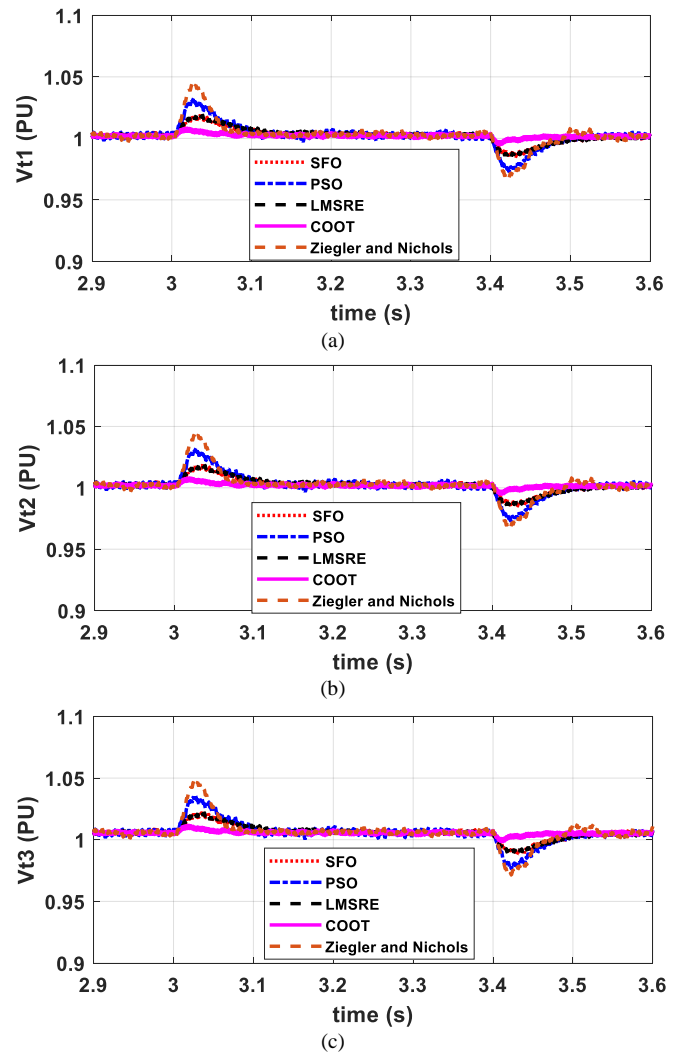


**FIGURE 8.** The Results of CBMO, SFO, PSO, Ziegler-Nichols and LMSRE for Scenario2. (a) Reference voltage of DG 1. (b) Reference voltage of DG 2. (c) Reference voltage of DG 3

**TABLE 9.** the Results of CBMO, SFO, PSO, Ziegler-Nichols and LMSRE for Scenario2

Point of compar.	COOT		LMSRE	SFO		PSO		Ziegler-Nichols	
Scenario 2 DG 1									
Optimum size	Y <sub>1</sub>	6.3 74	Online	Y <sub>1</sub>	6.4 689	Y <sub>1</sub>	1.9 22	Y <sub>1</sub>	1.5
	Y <sub>2</sub>	0.0 01		Y <sub>2</sub>	0.0 124 8	Y <sub>2</sub>	0.0 116	Y <sub>2</sub>	0.00 88
	Y <sub>3</sub>	2.5 4		Y <sub>3</sub>	2.2 791	Y <sub>3</sub>	2.3 12	Y <sub>3</sub>	1.6
	Y <sub>4</sub>	0.9 23		Y <sub>4</sub>	0.2 38	Y <sub>4</sub>	0.2 313	Y <sub>4</sub>	0.15 8
MPUS	0.49 %		1.89%	2.21%		3.31%		3.5 %	
MPOS	0.986 %		2.22%	2.972%		3.55%		4.4 %	
T <sub>set</sub>	zero		0.402 s	0.432 s		0.451 s		0.456 s	
E <sub>ss</sub>	0.38 %		0.43%	0.441%		0.481%		1.091 %	
Scenario 2 DG 2									
Optimum size	Y <sub>5</sub>	6.2 93	Online	Y <sub>5</sub>	6.0 241	Y <sub>5</sub>	1.4 023	Y <sub>5</sub>	0.98 5
	Y <sub>6</sub>	0.0 012		Y <sub>6</sub>	0.0 093	Y <sub>6</sub>	0.0 101	Y <sub>6</sub>	0.00 86
	Y <sub>7</sub>	2.5 11		Y <sub>7</sub>	1.8 61	Y <sub>7</sub>	1.7 981	Y <sub>7</sub>	1.55
	Y <sub>8</sub>	0.9 18		Y <sub>8</sub>	0.2 072	Y <sub>8</sub>	0.1 998	Y <sub>8</sub>	0.15 5
MPUS	0.492 %		1.88%	2.121%		3.2751%		3.48 %	
MPOS	0.963 %		2.2%	2.612%		3.642%		4.47 %	
T <sub>set</sub>	zero		0.403s	0.42892 s		0.4451 s		0.453 s	
E <sub>ss</sub>	0.392 %		0.52%	0.6651%		0.693%		0.985 %	
Scenario 2 DG 3									
Optimum size	Y <sub>9</sub>	6.1 43	Online	Y <sub>9</sub>	5.4 971	Y <sub>9</sub>	0.8 998	Y <sub>9</sub>	0.97
	Y <sub>10</sub>	0.0 013		Y <sub>10</sub>	0.0 067	Y <sub>10</sub>	0.0 654	Y <sub>10</sub>	0.00 82
	Y <sub>11</sub>	2.4 895		Y <sub>11</sub>	1.5 782	Y <sub>11</sub>	1.4 876	Y <sub>11</sub>	1.52
	Y <sub>12</sub>	0.8 95		Y <sub>12</sub>	0.1 751	Y <sub>12</sub>	0.1 622	Y <sub>12</sub>	0.15 1
MPUS	0.498 %		1.51%	1.746%		2.9091%		3.35 %	
MPOS	0.947 %		2.53%	2.62%		3.72%		4.485 %	
T <sub>set</sub>	zero		0.401s	0.4241 s		0.4431 s		0.464 s	
E <sub>ss</sub>	0.41 %		0.73%	1.033%		1.072%		1.12 %	

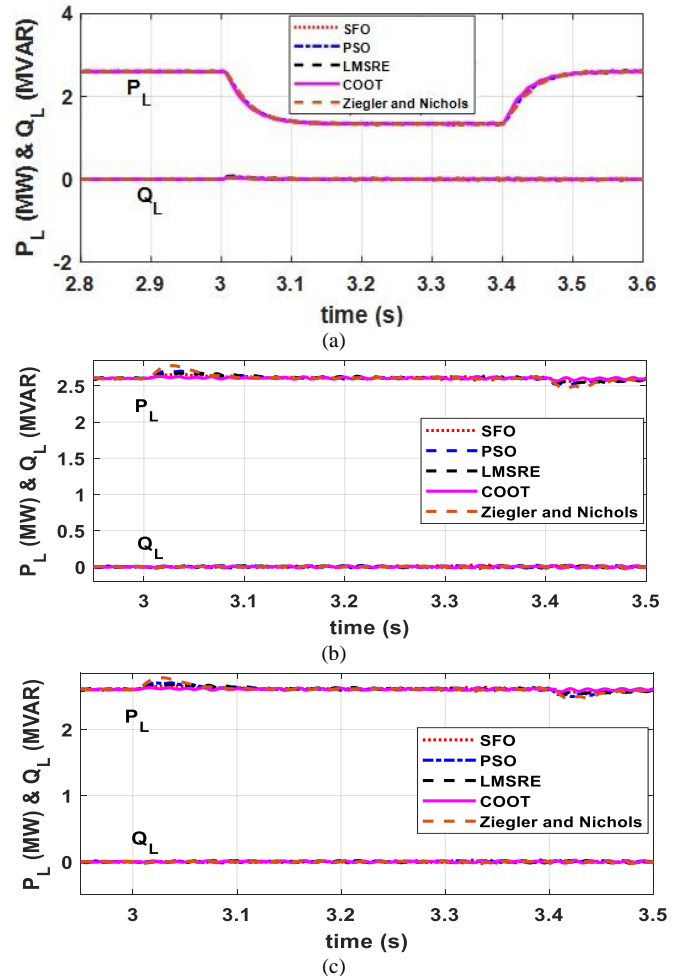


**FIGURE 9.** The Results of CBMO, SFO, PSO, Ziegler-Nichols and LMSRE for Scenario2. (a) Active and reactive load powers in DG 1. (b) Active and reactive load powers in DG 2. (c) Active and reactive load powers in DG 3.

**TABLE 10.** The Ziegler-Nichols Critical gains (k<sub>cr</sub>) and Critical periods (P<sub>cr</sub>) for the DGs for Scenario 3

	Critical gains (k <sub>cr</sub> )	Critical periods (P <sub>cr</sub> )	PI gains	
			Y <sub>i</sub>	PI gain
PI <sub>1,1</sub>	3.33	0.0102	Y <sub>1</sub>	1.5
			Y <sub>2</sub>	0.0085
PI <sub>2,1</sub>	4.44	0.1932	Y <sub>3</sub>	2
			Y <sub>4</sub>	0.161
PI <sub>2,1</sub>	3.1778	0.00984	Y <sub>5</sub>	1.43
			Y <sub>6</sub>	0.0082
PI <sub>2,2</sub>	4.3778	0.1824	Y <sub>7</sub>	1.97
			Y <sub>8</sub>	0.152
PI <sub>3,1</sub>	3.1333	0.00948	Y <sub>9</sub>	1.41
			Y <sub>10</sub>	0.0079
PI <sub>3,2</sub>	4.2667	0.1788	Y <sub>11</sub>	1.92
			Y <sub>12</sub>	0.149

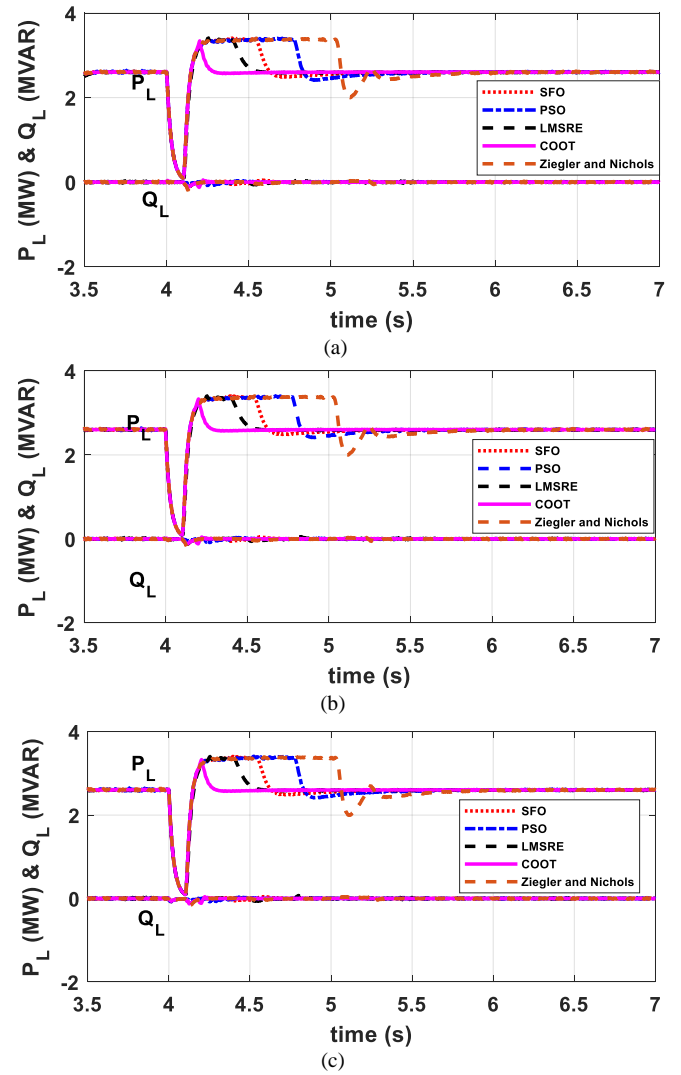
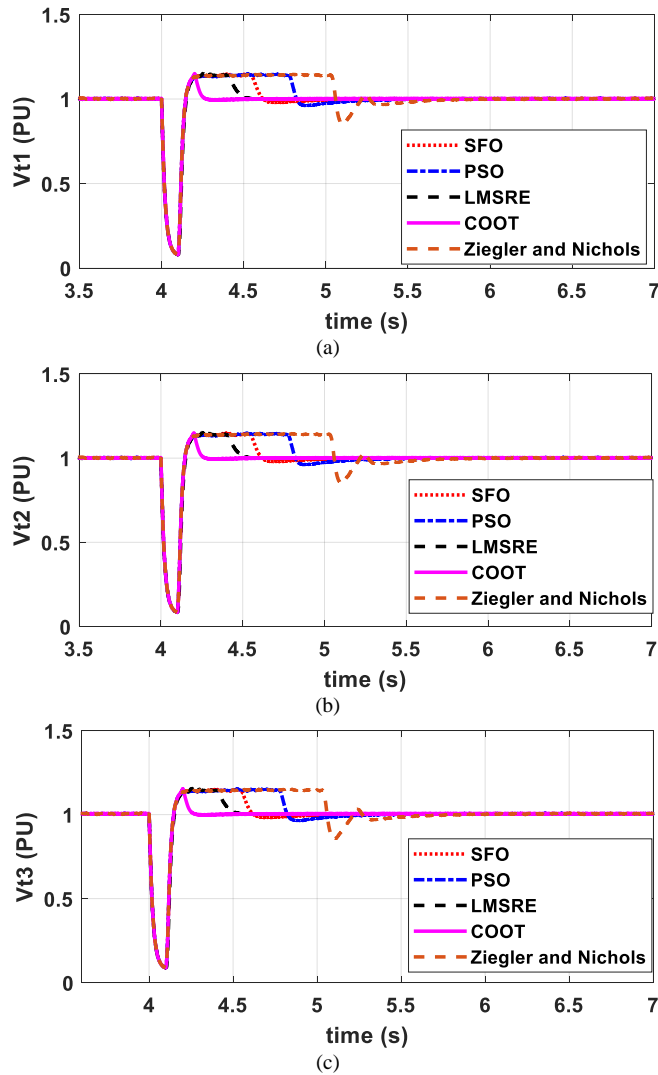


**FIGURE 10.** The Results of CBMO, SFO, PSO, Ziegler-Nichols and LMSRE for Scenario3. (a) Reference voltage of DG 1. (b) Reference voltage of DG 2. (c) Reference voltage of DG 3

**FIGURE 11.** The Results of CBMO, SFO, PSO, Ziegler-Nichols and LMSRE for Scenario3. (a) Active and reactive load powers in DG 1. (b) Active and reactive load powers in DG 2. (c) Active and reactive load powers in DG 3.

**Table 11. the Results of CBMO, SFO, PSO, Ziegler-Nichols and LMSRE for Scenario3**

Point of compar.	COOT		LMSRE	SFO		PSO		Ziegler-Nichols	
Scenario 3 DG 1									
Optimum size	Y <sub>1</sub>	6.5	online	Y <sub>1</sub>	6.13 41	Y <sub>1</sub>	2.10 81	Y <sub>1</sub>	1.5
	Y <sub>2</sub>	0.0 01		Y <sub>2</sub>	0.00 42	Y <sub>2</sub>	0.00 614	Y <sub>2</sub>	0.0 085
	Y <sub>3</sub>	2.6		Y <sub>3</sub>	2.49 81	Y <sub>3</sub>	2.57 2	Y <sub>3</sub>	2
	Y <sub>4</sub>	0.9		Y <sub>4</sub>	0.12 12	Y <sub>4</sub>	0.11	Y <sub>4</sub>	0.1 61
MPUS	92.11 %		92.17%	91.639%		93.109%		93.21%	
MPOS	11.55 %		12.41%	11.706%		11.9561%		12.31%	
T <sub>set</sub>	0.2447sec		0.491 s	0.56541 s		0.81 s		1.225 s	
E <sub>ss</sub>	0.31 %		0.251%	0.462%		0.551%		0.97%	
Scenario 3 DG 2									
Optimum size	Y <sub>5</sub>	6.3 65	online	Y <sub>5</sub>	6.21	Y <sub>5</sub>	2.17 7	Y <sub>5</sub>	1.4 3
	Y <sub>6</sub>	0.0 012		Y <sub>6</sub>	0.00 42	Y <sub>6</sub>	0.00 598	Y <sub>6</sub>	0.0 082
	Y <sub>7</sub>	2.5 86		Y <sub>7</sub>	2.51 2	Y <sub>7</sub>	2.55 1	Y <sub>7</sub>	1.9 7
	Y <sub>8</sub>	0.9 46		Y <sub>8</sub>	0.11 91	Y <sub>8</sub>	0.09 88	Y <sub>8</sub>	0.1 52
MPUS	91.61 %		91.68%	92.136%		92.141%		92.51%	
MPOS	11.65 %		12.40%	11.75%		11.62%		11.92%	
T <sub>set</sub>	0.2446 s		0.4917s	0.5721 s		0.8176 s		1.24 s	
E <sub>ss</sub>	0.324 %		0.337%	0.4952%		0.631%		0.99%	
Scenario 3 DG 3									
Optimum size	Y <sub>9</sub>	6.2 12	online	Y <sub>9</sub>	6.12	Y <sub>9</sub>	2.21	Y <sub>9</sub>	1.4 1
	Y <sub>10</sub>	0.0 013		Y <sub>10</sub>	0.00 41	Y <sub>10</sub>	0.00 61	Y <sub>10</sub>	0.0 079
	Y <sub>11</sub>	2.5 23		Y <sub>11</sub>	2.47 2	Y <sub>11</sub>	2.51	Y <sub>11</sub>	1.9 2
	Y <sub>12</sub>	0.9 67		Y <sub>12</sub>	0.12 1	Y <sub>12</sub>	0.01 06	Y <sub>12</sub>	0.1 49
MPUS	91.26 %		91.31%	93.1061%		91.641%		92.62%	
MPOS	12.1 %		12.82%	11.56%		11.53%		12.33%	
T <sub>set</sub>	0.249 sec		0.4973s	0.57541 s		0.824 s		1.27 s	
E <sub>ss</sub>	0.434 %		0.671%	0.8421%		1.022%		1.21%	

## VII. CONCLUSIONS

A new PI controller optimal design based on CMBO has been developed in this paper. The new proposal considers various PI controller parameters to enhance microgrid efficiency. The control method employs six PI controllers.

Extensive simulations were performed on a benchmark MG, with the aim of validating the developed methodology. The practicality of the control scheme is demonstrated by the simulation data, which is taken from the PSCAD/EMTDC software. The results evidenced that the proposed controller is able to keep stable the active and reactive powers simultaneously and effectively regulate the voltage profile. Results obtained also confirmed rapid damping in transient response with a quick T<sub>set</sub> and a slight E<sub>ss</sub> under several microgrid operating conditions, 1) isolating the system from the grid (autonomous mode), 2) islanded system exposure to load change, and 3) islanded system exposure to a 3 phase fault.

The suggested optimizer was validated by comparing its results with those achieved using the LMSRE-based adaptive control, SFO, Ziegler-Nichols, and the PSO techniques. In all the studied scenarios, CBMO attained lower values of the transient responses than those obtained via the LMSRE-based adaptive control, SFO, Ziegler-Nichols and the PSO techniques. More precisely, the CMBO was able to improve the voltage MPUS up to 74%, 77.8%, 85% and 86% compared with LMSRE-based adaptive control, SFO, Ziegler-Nichols and the PSO techniques, respectively. The new proposal was also able to reduce T<sub>set</sub> by 100% in scenario 2, when the MG suffers an abrupt load variation in off-grid mode.

The upcoming research will concentration on strengthening the presented CBMO based PI controller to modify the power system requests, energy storage strategies, and smart-grids, reaching optimal comebacks in the green energy systems.

VIII. APPENDIX

Table A1 PSCAD results for scenario 1

Exp.	K <sub>p1</sub>	T <sub>i1</sub>	K <sub>p2</sub>	T <sub>i2</sub>	N <sub>1</sub> MPUS <sub>1</sub> (%)	N <sub>3</sub> T <sub>set1</sub> (%)	N <sub>4</sub> E <sub>ss1</sub> (%)	N <sub>5</sub> MPUS <sub>2</sub> (%)	N <sub>7</sub> T <sub>set2</sub> (%)	N <sub>8</sub> E <sub>ss2</sub> (%)	N <sub>9</sub> MPUS <sub>1</sub> (%)	N <sub>11</sub> T <sub>set1</sub> (%)	N <sub>12</sub> E <sub>ss1</sub> (%)
1	0	0	0	0	14.871	0.141	0.7517	15.2631	0.1485	0.62	15.827	0.15988	0.6278
2	-1	1	1	1	26.512	0.1821	1.052	26.82	0.1847	0.7321	27.3	0.22021	1.02
3	1	1	1	1	12.231	0.28445	0.693	12.512	0.2984	0.512	12.92	0.34561	0.538
4	-1	-1	-1	-1	18.732	0.10571	0.283	19.11	0.10024	0.371	19.62	0.08641	1.044
5	1	0	0	0	11.573	0.16788	0.8	11.9162	0.17872	0.5391	12.38	0.19874	0.72086
6	-1	-1	1	1	30.221	0.29312	1.24	30.582	0.3263	0.9551	30.96	0.3761	0.387
7	0	0	0	0	14.872	0.141	0.7517	15.2632	0.1485	0.61	15.827	0.15988	0.6278
8	1	-1	-1	-1	11.412	0.07892	0.377	11.721	0.0796	0.361	12.07	0.0841	0.93
9	1	-1	1	1	14.321	0.26241	0.586	14.621	0.2789	0.4161	15.091	0.30932	0.658
10	0	0	0	1	14.942	0.14889	0.778	15.2881	0.151	0.5942	15.803	0.16811	0.448
11	0	0	0	-1	15.381	0.16251	0.483	15.732	0.15156	0.32	16.29	0.16522	0.9867
12	-1	1	1	-1	27.422	0.18172	0.514	27.721	0.18484	0.792	28.23	0.21531	1.54
13	0	0	0	0	14.871	0.141	0.7517	15.2632	0.1485	0.62	15.827	0.15988	0.6278
14	0	0	0	0	14.872	0.142	0.7517	15.2631	0.1485	0.62	15.827	0.15988	0.6278
15	1	1	-1	-1	9.341	0.0791	0.307	9.682	0.082	0.3652	10.1	0.09288	1.12
16	0	0	0	0	14.871	0.141	0.7517	15.2631	0.1485	0.62	15.827	0.15987	0.6278
17	1	1	-1	1	8.992	0.07672	0.565	9.3142	0.0794	0.38581	9.666	0.08977	0.701
18	-1	-1	-1	1	18.971	0.1061	0.664	19.42	0.1055	0.4752	19.81	0.09181	0.622
19	-1	0	0	0	23.62	0.11292	0.7733	23.962	0.1155	0.3171	24.54	0.12911	0.862
20	1	1	1	-1	12.5062	0.28441	0.185	12.792	0.3038	0.7382	13.2	0.35371	1.469
21	-1	1	-1	1	13.371	0.05141	0.6	13.72	0.0519	0.42	14.1	0.05641	0.725
22	0	0	0	0	14.871	0.142	0.7517	15.2631	0.1485	0.61	15.827	0.15986	0.6278
23	0	-1	0	0	13.681	0.13481	0.8	16.762	0.14	0.5842	17.34	0.14831	0.546
24	-1	-1	1	-1	30.311	0.1651	0.24	30.631	0.1954	0.511	31.08	0.24582	1.159
25	1	-1	-1	1	11.062	0.0792	1.69	11.371	0.9799	1.312	11.71	0.0852	0.73
26	1	-1	1	-1	14.251	0.27891	0.434	14.5361	0.29	0.732	14.96	0.34831	1.47
27	0	1	0	0	14.92	0.14571	0.71	15.251	0.15383	0.45661	15.856	0.17042	0.734
28	0	0	0	0	14.871	0.142	0.7517	15.2631	0.1485	0.62	15.827	0.15986	0.6278
29	-1	1	-1	-1	12.582	0.05961	0.204	12.892	0.0572	0.5262	13.25	0.06222	1.255
30	0	0	1	0	17.21	0.2373	0.719	17.5451	0.24578	0.5261	18.03	0.28211	0.57089
31	0	0	-1	0	10.612	0.07071	0.5522	10.912	0.0731	0.3092	11.305	0.08212	0.8378

Table A2 PSCAD results for scenario 2

Exp.	K <sub>p1</sub>	T <sub>i1</sub>	K <sub>p2</sub>	T <sub>i2</sub>	N <sub>1</sub> MPUS <sub>1</sub> (%)	N <sub>2</sub> MPOS <sub>1</sub> (%)	N <sub>3</sub> T <sub>set1</sub> (%)	N <sub>4</sub> E <sub>ss1</sub> (%)	N <sub>5</sub> MPUS <sub>1</sub> (%)	N <sub>6</sub> MPOS <sub>1</sub> (%)	N <sub>7</sub> T <sub>set1</sub> (%)	N <sub>8</sub> E <sub>ss1</sub> (%)	N <sub>9</sub> MPUS <sub>1</sub> (%)	N <sub>10</sub> MPOS <sub>1</sub> (%)	N <sub>11</sub> T <sub>set1</sub> (%)	N <sub>12</sub> E <sub>ss1</sub> (%)
1	0	0	0	0	2.9611	3.955	0.4783	0.266	3.221	3.516	0.49578	0.568	3.971	2.7	0.5871	1.48
2	-1	1	1	1	5.32	7.76	0.6458	0.422	5.332	7.197	0.65671	0.673	5.792	6.31	0.7317	1.3
3	1	1	1	1	2.372	4.16	0.4871	0.55	2.522	3.788	0.5068	0.8005	3.132	3.02	0.6177	1.49
4	-1	-1	-1	-1	4.341	5.143	0.4731	0.284	4.521	4.683	0.48211	0.416	5.2341	3.8	0.5098	1.47
5	1	0	0	0	2.2722	3.323	0.4621	0.207	2.5181	2.8879	0.48752	0.639	3.2822	2.119	0.592	1.48

6	-1	-1	1	1	5.651	7.67	0.6207	0.324	5.652	7.16	0.62921	0.105	5.992	6.36	0.6738	0.82
7	0	0	0	0	2.9612	3.955	0.4783	0.266	3.222	3.516	0.49578	0.568	3.971	2.7	0.5872	1.48
8	1	-1	-1	-1	3.1211	3.67	0.4731	0.461	3.361	3.19	0.4821	0.39	4.001	2.4	0.5123	1.311
9	1	-1	1	1	2.442	4.85	0.5068	0.178	2.592	4.5	0.51232	0.572	3.132	3.756	0.6065	1.173
10	0	0	0	1	2.81	4.07	0.4681	0.437	3.0091	3.64	0.4815	0.389	3.631	2.93	0.5065	1.11
11	0	0	0	-1	3.7281	4.37	0.5372	1.445	4.082	3.87	0.5598	1.742	5.1322	2.8	1.001	2.931
12	-1	1	1	-1	6.341	7.11	0.7292	0.98	6.522	6.6	0.792	1.49	7.362	5.56	1.12	0.45
13	0	0	0	0	2.9612	3.955	0.4781	0.266	3.221	3.516	0.49578	0.568	3.972	2.7	0.5871	1.48
14	0	0	0	0	2.9612	3.955	0.4783	0.266	3.221	3.516	0.49578	0.568	3.971	2.7	0.5873	1.48
15	1	1	-1	-1	3.151	3.88	0.4818	0.364	3.421	3.45	0.49312	0.634	4.261	2.57	0.5433	1.75
16	0	0	0	0	2.9612	3.955	0.4783	0.266	3.222	3.516	0.49578	0.568	3.971	2.7	0.5873	1.48
17	1	1	-1	1	2.741	3.92	0.4789	0.5	2.862	3.616	0.49272	0.173	3.371	2.916	0.5181	0.963
18	-1	-1	-1	1	4.232	5.29	0.4731	0.568	4.262	4.93	0.47387	0.28	4.672	4.25	0.4848	0.836
19	-1	0	0	0	4.521	6.595	0.5318	0.219	4.72	6.18	0.54282	0.838	5.362	5.324	0.5962	1.68
20	1	1	1	-1	3.872	4.73	0.7292	1.404	4.151	4.31	0.82681	1.912	5.091	3.31	1.311	2.16
21	-1	1	-1	1	3.781	5.25	0.4791	0.483	3.842	4.896	0.492	0.221	4.32	4.16	0.5122	0.98
22	0	0	0	0	2.962	3.955	0.4781	0.266	3.221	3.516	0.49578	0.568	3.971	2.7	0.5871	1.48
23	0	-1	0	0	3.051	4.1	0.4737	0.311	3.2892	3.66	0.492	0.52	4.002	2.895	0.5651	1.45
24	-1	-1	1	-1	6.242	6.85	0.6625	1.11	6.41	6.35	0.69572	1.57	7.11	5.359	1.21	1.75
25	1	-1	-1	1	3.142	4.82	0.4792	0.456	3.352	4.32	0.48732	0.2	3.772	3.62	0.5128	0.775
26	1	-1	1	-1	3.461	4.51	0.7151	1.41	3.722	4.1	0.91791	1.92	4.642	3.17	1.4212	3.56
27	0	1	0	0	2.922	3.84	0.4763	0.265	3.171	3.379	0.49851	0.794	3.981	2.536	0.5653	1.72
28	0	0	0	0	2.961	3.955	0.4783	0.266	3.222	3.516	0.49578	0.568	3.972	2.7	0.5871	1.48
29	-1	1	-1	-1	4.482	5.134	0.4792	0.3	4.71	4.64	0.49041	0.69	5.462	3.7	0.5232	1.77
30	0	0	1	0	3.651	6.09	0.5458	0.6358	3.822	5.72	0.56232	0.953	4.472	4.87	0.7898	1.77
31	0	0	-1	0	3.521	4.487	0.4822	0.541	3.631	4.09	0.49021	0.191	4.161	3.348	0.5178	0.9955

**Table A3 PSCAD results for scenario 3**

Exp.	K <sub>p1</sub>	T <sub>i1</sub>	K <sub>p2</sub>	T <sub>i2</sub>	N <sub>1</sub> MPUS <sub>1</sub> (%)	N <sub>2</sub> MPOS <sub>1</sub> (%)	N <sub>3</sub> T <sub>set1</sub> (%)	N <sub>4</sub> E <sub>ss1</sub> (%)	N <sub>5</sub> MPUS <sub>1</sub> (%)	N <sub>6</sub> MPOS <sub>1</sub> (%)	N <sub>7</sub> T <sub>set1</sub> (%)	N <sub>8</sub> E <sub>ss1</sub> (%)	N <sub>9</sub> MPUS <sub>1</sub> (%)	N <sub>10</sub> MPOS <sub>1</sub> (%)	N <sub>11</sub> T <sub>set1</sub> (%)	N <sub>12</sub> E <sub>ss1</sub> (%)
1	0	0	0	0	92.391	6.58	1.8858	0.3356	90.1121	6.244	1.6892	0.477	87.8061	5.52	1.1668	0.771
2	-1	1	1	1	92.292	7.42	3.001	0.328	90.001	7.12	2.6971	10020 00	87.631	6.55	2.1167	0.585
3	1	1	1	1	92.311	7.53	2.7861	0.4	90.002	7.2	2.681	0.9	87.662	6.634	2.1861	0.55
4	-1	-1	-1	-1	92.541	7.37	5.1351	1.7659	90.311	7.14	5.00341	1.498	88.0492	6.833	5.677	0.987
5	1	0	0	0	92.388	6.738	1.8363	0.4929	90.102	6.39	1.6862	0.351	87.792	5.68	1.161	0.807
6	-1	-1	1	1	92.293	7.28	6.9871	1.987	89.988	6.97	6.1541	0.799	87.6541	6.37	5.9986	1.45
7	0	0	0	0	92.391	6.58	1.8858	0.3356	90.111	6.244	1.6892	0.477	87.8062	5.52	1.1668	0.771
8	1	-1	-1	-1	92.443	7.89	4.31	0.95	90.181	7.7177	4.1341	1.09	87.882	7.38	4.51	0.899
9	1	-1	1	1	92.301	7.46	5.22	7.63	89.991	7.144	4.7651	6.99	87.642	6.53	4.5231	5.498
10	0	0	0	1	92.343	7.6	2.31	0.277	90.034	7.28	2.2221	0.288	87.712	6.659	2.0161	0.334
11	0	0	0	-1	92.676	3.76	0.5532	0.4198	90.51	3.349	0.52861	0.3333	88.2541	2.3	0.4781	0.192
12	-1	1	1	-1	92.581	4.77	0.6891	0.53	90.37	4.4	0.6172	1.2	88.11	3.5	0.5284	923.4
13	0	0	0	0	92.392	6.58	1.8858	0.3356	90.1121	6.244	1.6892	0.477	87.8062	5.52	1.1668	0.771
14	0	0	0	0	92.392	6.58	1.8858	0.3356	90.1121	6.244	1.6892	0.477	87.8062	5.52	1.1668	0.771



15	1	1	-1	-1	92.541	7.8	3.2021	0.274	90.321	7.61	3.20271	0.457	88.041	7.19	3.2027	0.355
16	0	0	0	0	92.391	6.58	1.8858	0.3356	90.1121	6.244	1.6892	0.477	87.8062	5.52	1.1668	0.771
17	1	1	-1	1	92.32	8.17	6.22	4.56	89.994	7.91	6.0781	8.76	87.6651	7.49	5.9871	6.76
18	-1	-1	-1	1	92.291	8.07	7.1361	1.87	89.974	7.8	7.0571	1.43	87.6431	7.339	7.451	0.993
19	-1	0	0	0	92.381	6.9	2.1081	0.559	90.074	6.57	2.0412	0.506	87.7581	5.9	1.3193	0.44
20	1	1	1	-1	92.571	4.6	0.6222	0.51	90.351	4.21	0.57482	0.35	88.0851	3.29	0.4866	0.375
21	-1	1	-1	1	92.32	7.88	7.1761	8.033	89.981	7.61	6.8542	7.995	87.642	7.239	6.3608	8.12
22	0	0	0	0	92.391	6.58	1.8858	0.3356	90.1121	6.244	1.6892	0.477	87.8062	5.52	1.1668	0.771
23	0	-1	0	0	92.412	6.59	2.3361	0.249	90.132	6.25	2.2111	0.371	87.8021	5.539	1.6638	0.332
24	-1	-1	1	-1	92.552	4.77	0.8888	0.51	90.332	4.41	0.81382	0.46	88.031	3.5	0.6031	0.68
25	1	-1	-1	1	92.292	8.42	6.671	1.78	89.981	8.13	6.482	0.9876	87.662	7.69	6.7061	2.56
26	1	-1	1	-1	92.581	4.94	0.7418	0.75	90.372	4.54	0.69191	0.87	88.0812	3.61	0.5291	1.2
27	0	1	0	0	92.427	6.7	1.5362	0.345	90.1491	6.36	1.4612	0.285	87.8231	5.65	0.9862	0.471
28	0	0	0	0	92.391	6.58	1.8858	0.3356	90.1122	6.244	1.6892	0.477	87.8062	5.52	1.1668	0.771
29	-1	1	-1	-1	92.552	7.7	6.872	5.6	90.331	7.539	6.5671	5.1	88.051	7.08	6.1261	6.1
30	0	0	1	0	92.382	7.19	2.3611	4.52	90.0742	6.86	2.2131	0.347	87.7421	6.18	1.6381	0.525
31	0	0	-1	0	92.3451	8.03	5.002	7.44	90.0471	7.763	4.91	5.5	87.7271	7.278	4.61	3.25

Table A4 RSM model constants for Scenario 1 .

Cons.	scenario (1)									
	$N_1$	$N_3$	$N_4$	$N_5$	$N_7$	$N_8$	$N_9$	$N_{11}$	$N_{12}$	
M <sub>1</sub>	14.7832	0.14125	0.74541	-0.0094	0.14012	0.5251	15.8961	0.16001	0.62901	
M <sub>2</sub>	-5.3351	0.01859	0.00371	-5.351	0.06942	0.0155	-5.3771	0.02356	-0.01542	
M <sub>3</sub>	-1.3951	-0.00882	-0.08242	-1.559	-0.06111	-0.0448	-1.5572	-0.00936	0.08642	
M <sub>4</sub>	3.8842	0.08121	0.02342	3.869	0.03881	0.0781	3.8971	0.10921	0.04711	
M <sub>5</sub>	-0.0731	0.00490	0.26891	-0.067	0.05622	0.0605	-0.0802	0.00491	-0.28581	
M <sub>6</sub>	2.9052	-0.0023	0.0492	2.521	0.01681	-0.010	2.4841	0.0038	0.16112	
M <sub>7</sub>	-0.3911	-0.0025	0.0171	0.588	0.01661	0.083	0.6222	-0.0008	0.00961	
M <sub>8</sub>	-0.7762	0.0112	-0.1022	-1.190	0.02912	-0.020	-1.3081	0.0220	0.07401	
M <sub>9</sub>	0.4792	0.0130	-0.1072	0.092	0.02102	0.009	0.0712	0.0065	0.08702	
M <sub>10</sub>	0.6482	0.01378	-0.08002	0.665	-0.03852	-0.0597	0.6652	0.01883	-0.08052	
M <sub>11</sub>	-2.3941	0.01857	-0.14601	-2.392	-0.03911	-0.0777	-2.3851	0.01529	0.01212	
M <sub>12</sub>	-0.0591	-0.00870	-0.00521	-0.066	0.04692	0.0039	-0.0581	-0.01149	-0.00741	
M <sub>13</sub>	0.3411	0.00225	0.08012	0.341	0.05471	0.0623	0.3532	-0.00617	0.02611	
M <sub>14</sub>	-0.0391	-0.00765	-0.07162	-0.046	-0.06492	-0.0986	-0.0402	-0.00686	-0.01211	
M <sub>15</sub>	-0.0962	0.00763	-0.00941	-0.098	-0.04901	-0.0690	-0.0901	0.00566	-0.09152	

Table A5 RSM model constants for Scenario 2

Cons.	scenario (2)											
	$N_1$	$N_2$	$N_3$	$N_4$	$N_5$	$N_6$	$N_7$	$N_8$	$N_9$	$N_{10}$	$N_{11}$	$N_{12}$
M <sub>1</sub>	3.00021	4.118	0.477791	0.3454	3.25181	3.683	0.49321	0.6417	4.00412	2.866	0.59591	1.572
M <sub>2</sub>	-1.01772	-1.0522	-0.015622	0.0467	-0.96842	-1.0263	-0.0024	0.0532	-0.9217	-0.9968	0.01671	0.2003
M <sub>3</sub>	-0.04001	-0.0622	0.006102	0.0092	-0.03492	-0.0565	0.00422	0.0786	0.01142	-0.0849	-0.00361	-0.0312
M <sub>4</sub>	0.37892	0.6742	0.074551	0.1698	0.37561	0.6617	0.09531	0.3778	0.41531	0.6084	0.21201	0.2013
M <sub>5</sub>	-0.34881	0.1329	-0.03558	-0.2133	-0.41452	0.1586	-0.0558	-0.4084	-0.5832	0.2585	-0.16421	-0.4281
M <sub>6</sub>	0.3502	0.650	0.01972	-0.2250	0.3201	0.655	0.02501	0.011	0.27721	0.662	-0.01302	-0.099
M <sub>7</sub>	-0.0612	-0.339	-0.00231	-0.1500	-0.0591	-0.359	0.00411	-0.071	-0.05382	-0.344	-0.04071	-0.094
M <sub>8</sub>	0.5392	0.980	0.03662	0.1504	0.4361	1.026	0.03612	-0.156	0.27121	1.050	0.04782	-0.296
M <sub>9</sub>	0.2181	-0.089	0.02522	0.5030	0.2562	-0.124	0.03051	0.338	0.33721	-0.194	0.14731	0.341
M <sub>10</sub>	0.03312	-0.0913	-0.006272	0.0259	0.02312	-0.0723	-0.0142	-0.0166	0.02461	-0.0682	-0.00391	-0.005
M <sub>11</sub>	-0.41941	-0.4133	-0.014261	0.0350	-0.41191	-0.3773	-0.0015	0.0985	-0.37412	-0.3706	0.01211	0.270
M <sub>12</sub>	-0.02942	-0.0483	-0.020161	-0.0674	-0.01692	-0.0460	-0.0322	-0.0140	-0.01161	-0.0499	-0.03752	-0.180
M <sub>13</sub>	0.04811	0.0387	0.004061	0.0285	0.05191	0.0191	-0.0011	0.0173	0.04962	0.0174	-0.01372	-0.186
M <sub>14</sub>	-0.12192	-0.1388	-0.005262	0.0404	-0.13062	-0.1306	0.00131	0.0175	-0.13542	-0.1244	0.01682	0.193
M <sub>15</sub>	-0.18441	-0.0133	-0.036151	-0.2518	-0.18811	-0.0321	-0.0575	-0.2178	-0.20661	-0.0268	-0.14621	-0.024

Table A6 RSM model constants for Scenario 3

Cons.	scenario (3)											
	$N_1$	$N_2$	$N_3$	$N_4$	$N_5$	$N_6$	$N_7$	$N_8$	$N_9$	$N_{10}$	$N_{11}$	$N_{12}$
M <sub>1</sub>	92.4011	6.582	1.776	0.8221	90.1205	6.238	1.631	0.493	87.8113	5.507	1.103	-6.81
M <sub>2</sub>	-0.00283	0.0771	-0.469	-0.214	-0.00338	0.073	-0.418	0.088	-0.00295	0.067	-0.384	-51.31
M <sub>3</sub>	-0.00273	-0.0121	-0.4062	0.1721	0.012891	-0.0081	-0.3652	0.5981	0.01412	-0.008	-0.538	51.82
M <sub>4</sub>	0.01450	-0.8541	-1.578	-0.838	0.01912	-0.9091	-1.6152	-1.151	0.01488	-1.076	-1.779	50.21
M <sub>5</sub>	0.00954	0.9021	1.3592	0.8641	-0.17268	0.9032	1.2701	0.946	-0.20371	0.9902	1.1781	-50.42
M <sub>6</sub>	-0.0293	0.2361	0.3272	-0.865	-0.0424	0.2462	0.3021	-0.082	-0.0434	0.2991	0.2132	16.32
M <sub>7</sub>	0.0146	0.0621	0.2912	-1.094	0.0093	0.072	0.275	-0.182	-0.0049	0.1041	0.2981	16.01
M <sub>8</sub>	-0.0513	1.0272	2.0351	4.592	-0.06981	1.0782	1.9951	2.415	-0.08281	1.2382	2.0931	17.52
M <sub>9</sub>	-0.12807	-0.9031	-0.2192	-1.043	0.1373	-0.9191	-0.1862	-0.198	0.16471	-1.012	0.2212	15.91
M <sub>10</sub>	0.00363	-0.0561	-0.1061	-0.859	0.004811	-0.0592	-0.0781	-0.613	0.00907	-0.059	0.014	-58.51
M <sub>11</sub>	-0.0292	-0.0612	0.2334	0.9771	0.00957	-0.0688	0.2512	0.6981	0.01182	-0.071	0.2312	-57.12
M <sub>12</sub>	0.00725	0.0191	0.0801	0.5052	0.008312	0.0182	0.1022	0.7931	0.01257	0.0181	0.1062	58.31
M <sub>13</sub>	0.0053	0.00412	-0.4332	-1.328	-0.00919	-0.0011	-0.3682	-1.486	-0.00582	0.0131	-0.231	56.32
M <sub>14</sub>	-0.00651	-0.0083	-0.4473	-0.182	-0.00795	-0.0102	-0.4042	0.2792	-0.01483	0.0152	-0.443	-57.61
M <sub>15</sub>	-0.0512	0.5521	0.462	0.0241	-0.01395	0.5893	0.3772	-0.315	-0.01883	0.684	0.357	-58.1

## IX. REFERENCES

- [1] Menesy, Ahmed S., Hamdy M. Sultan, Salah Kamel, Rania A. Turkey, Ahmed Al-Durra, and Hany M. Hasanien. "Optimal Values of Unknown Parameters of Polymer Electrolyte Membrane Fuel Cells Using Improved Chaotic Electromagnetic Field Optimization." In 2020 IEEE Industry Applications Society Annual Meeting, pp. 1-8. IEEE, 2020.
- [2] Soliman, Mahmoud A., et al. "High performance frequency converter controlled variable-speed wind generator using linear-quadratic regulator controller." IEEE Transactions on Industry Applications 56.5 (2020): 5489-5498.
- [3] Alsaidan, Ibrahim, et al. "Proton Exchange Membrane Fuel Cells Modeling Using Chaos Game Optimization Technique." Sustainability 13.14 (2021): 7911.
- [4] Shaheen, Mohamed AM, et al. "Precise modeling of PEM fuel cell using improved chaotic MayFly optimization algorithm." International Journal of Energy Research (2021), Enlist.
- [5] Soliman, Mahmoud A., et al. "An adaptive fuzzy logic control strategy for performance enhancement of a grid-connected PMSG-based wind turbine." IEEE Transactions on Industrial Informatics 15.6 (2018): 3163-3173.
- [6] Hussien, Ahmed M., et al. "LMSRE-Based Adaptive PI Controller for Enhancing the Performance of an Autonomous Operation of Microgrids." IEEE Access 9 (2021): 90577-90586.
- [7] D. Kumar, H. D. Mathur, S. Bhanot, and R. C. Bansal, "Forecasting of solar and wind power using LSTM RNN for load frequency control in isolated microgrid", International Journal of Modelling and Simulation, vol. 41, no. 4, 2021, 311-323.
- [8] T. Adefarati, R. C. Bansal, M. Bettayeb, and R. Naidoo, "Optimal energy management of a PV-WTG-BSS-DG microgrid system", Energy, vol. 217, no. 119538, pp. 1-21, 2021.
- [9] A. Sujil, R. Kumar and R.C. Bansal, "An intelligent multi agent based approach for autonomous energy management in a microgrid", Electric Power Components and Systems, vol. 49, no. 1-2, pp. 18-31, 2021.
- [10] Taher, Ahmed M., et al. "Hierarchical Model Predictive Control for Performance Enhancement of Autonomous Microgrids." Ain Shams Engineering Journal (2021), Enlist.
- [11] Kumar, Abhinandan, and Tirthadip Ghose. "A Newton-Raphson-based unified load flow of grid-connected and islanded AC-DC microgrids." International Transactions on Electrical Energy Systems (2021): e13075.
- [12] D. N. Gaonkar, and J. M. Guerrero, "Improved Pf/QV and PV/Qf droop controllers for parallel distributed generation inverters in AC microgrid," Sustain. Cities Soc., Vol. 41, pp. 421-442, Aug. 2018.
- [13] An, Ronghui, et al. "A Comprehensive Solution to Decentralized Coordinative Control of Distributed Generations in Islanded Microgrid Based on Dual-Frequency-Droop." IEEE Transactions on Power Electronics (2021), Enlist.
- [14] Ozkan, Ziya, and Ahmet Hava. "Inductor Saturation Compensation in Three-Phase Three-Wire Voltage-Source Converters via Inverse System Dynamics." IEEE Transactions on Industrial Electronics (2021), Enlist.
- [15] D'Arco, Salvatore, Jon Are Suul, and Olav Bjarte Fosso. "Automatic tuning of cascaded controllers for power converters using eigenvalue parametric sensitivities." IEEE Transactions on Industry Applications 51.2 (2014): 1743-1753.
- [16] Saleh, Mahmoud, Yusef Esa, and Ahmed Mohamed. "Centralized control for DC microgrid using finite state machine." In 2017 IEEE Power & Energy Society Innovative Smart Grid Technologies Conference (ISGT), pp. 1-5. IEEE, 2017.
- [17] Wang, William SW, Daniel E. Davison, and Edward J. Davison. "Controller design for multivariable linear time-invariant unknown systems." IEEE Transactions on Automatic Control 58.9 (2013): 2292-2306.
- [18] Bhatshvar, Y. K., and H. D. Mathur. "Power-frequency balance with superconducting magnetic energy storage using optimized intelligent controller." Energetika 60.3 (2014).
- [19] Hussien, A. M., Hany M. Hasanien, and S. F. Mekhamer. "Sunflower optimization algorithm-based optimal PI control for enhancing the performance of an autonomous operation of a microgrid." Ain Shams Engineering Journal 12.2 (2021): 1883-1893.
- [20] Patel, Sunita, Banaja Mohanty, and Hany M. Hasanien. "Competition over resources optimized fuzzy TIDF controller for frequency stabilization of hybrid micro-grid system." International Transactions on Electrical Energy Systems 30.9 (2020): e12513.
- [21] Ambia, Mir Nahidul, et al. "Harmony search algorithm-based controller parameters optimization for a distributed-generation system." IEEE Transactions on Power Delivery 30.1 (2014): 246-255.
- [22] Hussien, A. M., S. F. Mekhamer, and Hany M. Hasanien. "Cuttlefish optimization algorithm based optimal PI controller for performance enhancement of an autonomous operation of a DG system." In 2020 2nd International Conference on Smart Power & Internet Energy Systems (SPIES), pp. 293-298. IEEE, 2020.
- [23] Shaheen, Mohamed AM, Hany M. Hasanien, and Ahmed Al-Durra. "Solving of Optimal Power Flow Problem Including Renewable Energy Resources Using HEAP Optimization Algorithm." IEEE Access 9 (2021): 35846-35863.
- [24] Hassan, Nada Mamdouh, et al. "Toward centralized/decentralized controlled power flow applying whale versus genetic optimization algorithms." Int. J. Recent Tech. Eng. 8.4 (2019): 1-8.
- [25] Shaheen, Mohamed AM, et al. "Optimal power flow of power systems including distributed generation units using sunflower optimization algorithm." IEEE Access 7 (2019): 109289-109300.
- [26] Shaheen, Mohamed AM, S. F. Mekhamer, Hany M. Hasanien, and Hossam EA Talaat. "Optimal power flow of power systems using hybrid firefly and particle swarm optimization technique." In 2019 21st International Middle East Power Systems Conference (MEPCON), pp. 232-237. IEEE, 2019.
- [27] Qais, Mohammed, Hany M. Hasanien, and Saad Alghuwainem. "Salp swarm algorithm-based TS-FLCs for MPPT and fault ride-through capability enhancement of wind generators." ISA transactions 101 (2020): 211-224.
- [28] Shaheen, Mohamed AM, et al. "A novel application of improved marine predators algorithm and particle swarm optimization for solving the ORPD problem." Energies 13.21 (2020): 5679.
- [29] Mahmoud, Hassan Y., et al. "Hybrid cuckoo search algorithm and grey wolf optimiser-based optimal control strategy for performance enhancement of HVDC-based offshore wind farms." IET Generation, Transmission & Distribution 14.10 (2020): 1902-1911.
- [30] Abd Elmomen, Amany Hamdy, Hany M. Hasanien, and A. Y. Abdelaziz. "Development of Optimal PI controllers of an Inverter-Based Decentralized energy generation System Based on Equilibrium Optimization Algorithm." International Journal

of Renewable Energy Research (IJRER) 11.3 (2021): 1095-1106.

- [31] Swief, R. A., et al. "AC&DC optimal power flow incorporating centralized/decentralized multi-region grid control employing the whale algorithm." *Ain Shams Engineering Journal* 12.2 (2021): 1907-1922.
- [32] A. E. Chaib, H. R. E-H. Bouchekara, R. Mehasni, M. A. Abido, "Optimal power flow with emission and non-smooth cost functions using backtracking search optimization algorithm," *Int. J. Electr. Power Energy Syst.*, vol. 81, pp. 64-77, 2016.
- [33] H. M. Hasanien, A. S. Abd-Rabou, and S. M. Sakr, "Design optimization of transverse flux linear motor for weight reduction and performance improvement using response surface methodology and genetic algorithms," *IEEE Trans. Energy Convers.*, vol. 25, no. 3, pp. 598–605, Sep. 2010.
- [34] I. Y. Kim, O. L. de Weck, "Adaptive weighted sum method for multi-objective optimization: a new method for Pareto front generation", *Structural and Multidisciplinary Optimization*, Feb. 2006, Vol. 31, Issue 2, pp 105–116.
- [35] Qais, Mohammed H., Hany M. Hasanien, and Saad Alghuwainem. "A novel LMSRE-based adaptive PI control scheme for grid-integrated PMSG-based variable-speed wind turbine." *International Journal of Electrical Power & Energy Systems* 125: 106505.
- [36] Katsuhiko, Ogata. *Modern control engineering*. 2010.
- [37] Naruei, Iraj, and Farshid Keynia. "A New Optimization Method Based on Coot Bird Natural Life Model." *Expert Systems with Applications* (2021): 115352.
- [38] McNair D, Cramer-Burke C. Breeding ecology of American and Caribbean coots at Southgate Pond, St. Croix: Use of Woody Vegetation. *Wilson J. Ornithology* 2006;118(2):208-217, doi: 10.1676/05-020.1.
- [39] Shizuka D, Lyon B. Coots use hatch order to learn to recognize and reject conspecific brood parasitic chicks. *Nature*, 2010;463(7278):223-226, doi: 10.1038/nature08655.
- [40] Lukeman R, Li Y, Edelman-Keshet L. Inferring individual rules from collective behavior. *Proc. of the Nat. Acad. Sci. of USA*, 107;28:12576-12580, doi: 10.1073/pnas.1001763107.



**A.M. HUSSIEN** received his B.Sc. degree in Electrical Engineering from Future University In Egypt, Faculty of Engineering, Cairo, Egypt, in 2014. From 2014, he is M.Sc student at Ain Shams University, Faculty of Engineering, Cairo, Egypt. Currently, he is TA at Future University in Egypt, Faculty of Engineering, Cairo, Egypt. His research interests include power systems operation, Microgrid, renewable energy systems.



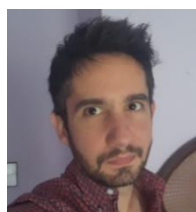
**RANIA A. TURKY** received his B.Sc. and M.Sc. degrees in Electrical Power Engineering from Ain Shams University, Faculty of Engineering, Cairo, Egypt, in 2004 and 2010, respectively. She is now pursuing PhD degree at Ain Shams University. Her research interests include modern control techniques, power systems dynamics and control, energy storage systems, renewable energy systems, and smart grid.



**Abdulaziz Alkuhayli** (S'11–M'19) received the B.Sc. degree in electrical engineering from King Saud University, Riyadh, Saudi Arabia, in 2006, the M.S. in electrical engineering from Missouri University of Science and Technology, Rolla, MO, USA, in 2013, and the Ph.D. degree in electrical engineering from North Carolina State University, Raleigh, NC, USA, in 2018. From 2006-2009, he worked as an Operation Engineer at the Energy Control Center, Saudi Electricity Company. He is currently an Assistant Professor with the Department of Electrical Engineering, King Saud University, Riyadh, Saudi Arabia. His research interests include energy management, renewable energy systems, flexible AC transmission systems, power system stability and smart grid.



**HANY M. HASANIEN** (M 09, SM 11) received his B.Sc., M.Sc. and Ph.D. degrees in Electrical Engineering from Ain Shams University, Faculty of Engineering, Cairo, Egypt, in 1999, 2004, and 2007, respectively. From 2008 to 2011, he was a Joint Researcher with Kitami Institute of Technology, Kitami, Japan. From 2012 to 2015, he was Associate Professor at College of Engineering, King Saud University, Riyadh, Saudi Arabia. Currently, he is Professor at the Electrical Power and Machines Department, Faculty of Engineering, Ain Shams University. His research interests include modern control techniques, power systems dynamics and control, energy storage systems, renewable energy systems, and smart grid. Prof. Hasanien is an Editorial Board Member of *Electric Power Components and Systems Journal*. He is Subject Editor of *IET Renewable Power Generation*, *Ain Shams Engineering Journal* and *Electronics MDPI*. He has authored, co-authored, and edited three books in the field of electric machines and renewable energy. He has published more than 150 papers in international journals and conferences. His biography has been included in *Marquis Who's Who in the world* for its 28 edition, 2011. He was awarded Encouraging Egypt Award for Engineering Sciences in 2012. He was awarded Institutions Egypt Award for Invention and Innovation of Renewable Energy Systems Development in 2014. He was awarded the Superiority Egypt Award for Engineering Sciences in 2019. Currently, he is IEEE PES Egypt Chapter Chair and Editor in Chief of *Ain Shams Engineering Journal*.



**MARCOS TOSTADO-VÉLIZ** received his B.Sc., (with Hons.) and M.Sc. degrees from University of Seville in 2016 and 2017, respectively. He received his Ph.D. degree in 2020, from University of Jaén. Currently, he is an assistant professor at the Electrical Engineering department of University of Jaén. His primary research interests include the applicability of numerical algorithms for power system analysis, energy management in microgrids, home energy management tools and application of metaheuristic optimizers.



**FRANCISCO JURADO** (Senior Member, IEEE) was born in Linares, Jaén, Spain. He received the M.Sc. and Dr. Ing. degrees from the National University of Distance Education, Madrid, Spain, in 1995 and 1999, respectively. Since 1985, he has been a Professor with the Department of Electrical Engineering, University of Jaén, Jaén. His current research interests include power systems, modeling, and renewable energy.



**Ramesh C. Bansal** has more than 25 years of diversified experience of research, scholarship of teaching and learning, accreditation, industrial, and academic leadership in several countries. Currently he is a Professor in the Department of Electrical Engineering at University of Sharjah and extraordinary professor at University of Pretoria. Previously he was

Professor and Group Head (Power) in the ECE Department at University of Pretoria (UP), South Africa. Prior to his appointment at UP, he was employed by the University of Queensland, Australia; University of the South Pacific, Fiji; BITS Pilani, India; and Civil Construction Wing, All India Radio. Prof. Bansal has significant experience of collaborating with industry and Government organizations. These utilities include NTPC (a 60 GW Indian power generation company), Powerlink, and ESKOM. He has made significant contribution to the development and delivery of BS and ME programmes for Utilities. He has extensive experience in the design and delivery of CPD programmes for professional engineers. He has carried out research and consultancy and attracted significant funding from Industry and Government Organisations. Prof. Bansal has published over 350 journal articles, presented papers at conferences, books, and chapters in books. He has Google citations of over 12000 and h-index of 50. He has supervised 25 PhD, 4 Post Docs and current supervising 5 Ph.D. students. His diversified research interests are in the areas of Renewable Energy (wind, PV, microgrid), Power Systems, and Smart Grid. Professor Bansal is an Editor/Associate Editor of several highly regarded journals including IEEE Systems Journal, IET Renewable Power Generation, and Technology and Economics of Smart Grids and Sustainable Energy. He is a Fellow and Chartered Engineer IET-UK, Fellow Institution of Engineers (India), and Senior Member of IEEE-USA.